Neuron

Article

Mechanical Allodynia Circuitry in the Dorsal Horn Is Defined by the Nature of the Injury

Graphical Abstract

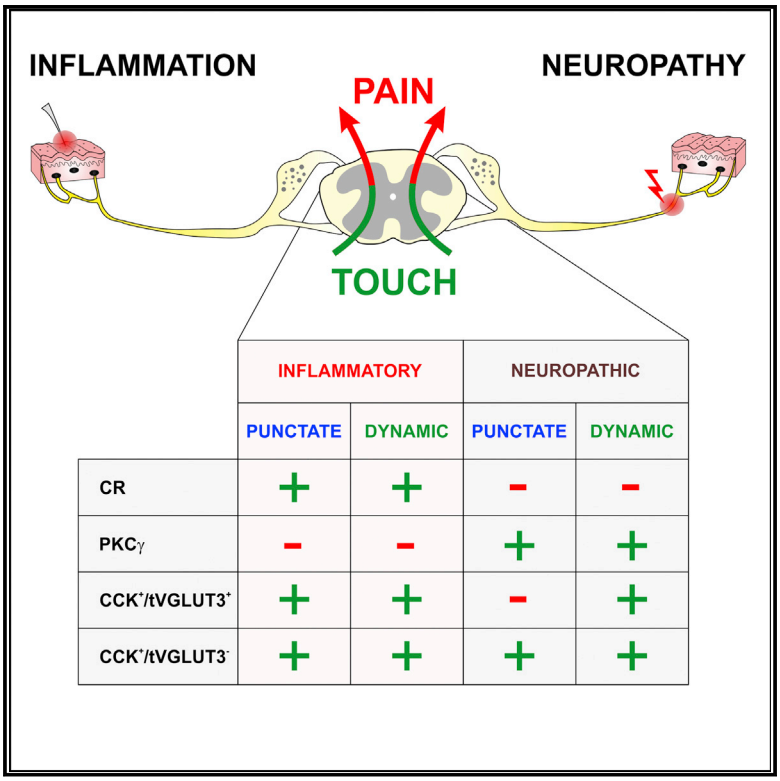

	INFLAMMATORY		NEUROPATHIC	
	PUNCTATE	DYNAMIC	PUNCTATE	DYNAMIC
CR	+	+	-	-
PKCγ	-	-	+	+
CCK⁺/tVGLUT3⁺	+	+	-	+
CCK⁺/tVGLUT3⁻	+	+	+	+

Authors

Cedric Peirs, Sean-Paul G. Williams, Xinyi Zhao, ..., Sarah E. Ross, Martyn Goulding, Rebecca P. Seal

Correspondence

rpseal@pitt.edu

In Brief

Peirs et al. identified distinct spinal cord microcircuits that underlie mechanical allodynia, depending on the injury type. The neurons engaged after neuropathic or inflammatory injuries include populations that express CCK, tVGLUT3, CR, and PKCγ.

Highlights

- CR neurons are important for mechanical allodynia in inflammatory injuries
- PKCγ neurons are important for mechanical allodynia in neuropathic injuries
- CCK and tVGLUT3 neurons in deeper laminae convey both types of injuries
- The *Maf*⁺ subset of CCK neurons encompasses tVGLUT3 and conveys dynamic allodynia

Peirs et al., 2021, Neuron *109*, 73–90
January 6, 2021
https://doi.org/10.1016/j.neuron.2020.10.027

CellPress

Neuron

CellPress

Article

Mechanical Allodynia Circuitry in the Dorsal Horn Is Defined by the Nature of the Injury

Cedric Peirs,[1,2,5,7] Sean-Paul G. Williams,[1,2,7] Xinyi Zhao,[1,2,6,7] Cynthia M. Arokiaraj,[1,2,8] David W. Ferreira,[1,2,8] Myung-chul Noh,[1,2] Kelly M. Smith,[1,2] Priyabrata Halder,[1,2] Kelly A. Corrigan,[1,2] Jeremy Y. Gedeon,[1,2] Suh Jin Lee,[1,2] Graziana Gatto,[3] David Chi,[4] Sarah E. Ross,[1,2] Martyn Goulding,[3] and Rebecca P. Seal[1,2,4,9,*]

[1]Department of Neurobiology, University of Pittsburgh School of Medicine, Pittsburgh, PA 15260, USA
[2]Pittsburgh Center for Pain Research, University of Pittsburgh School of Medicine, Pittsburgh, PA 15260, USA
[3]Molecular Neurobiology Laboratory, The Salk Institute for Biological Studies, 10010 North Torrey Pines Rd, La Jolla, CA 92037, USA
[4]Department of Otolaryngology, University of Pittsburgh School of Medicine, Pittsburgh, PA 15260, USA
[5]Present address: Université Clermont Auvergne, CHU, Clermont-Ferrand, Inserm, Neuro-Dol, Clermont-Ferrand F-63000, France.
[6]Present address: Department of Neurology, Beijing Tsinghua Changgung Hospital, School of Medicine, Tsinghua University, Beijing 102218, China
[7]These authors contributed equally
[8]These authors contributed equally
[9]Lead Contact
*Correspondence: rpseal@pitt.edu
https://doi.org/10.1016/j.neuron.2020.10.027

SUMMARY

The spinal dorsal horn is a major site for the induction and maintenance of mechanical allodynia, but the circuitry that underlies this clinically important form of pain remains unclear. The studies presented here provide strong evidence that the neural circuits conveying mechanical allodynia in the dorsal horn differ by the nature of the injury. Calretinin (CR) neurons in lamina II inner convey mechanical allodynia induced by inflammatory injuries, while protein kinase C gamma (PKCγ) neurons at the lamina II/III border convey mechanical allodynia induced by neuropathic injuries. Cholecystokinin (CCK) neurons located deeper within the dorsal horn (laminae III–IV) are important for both types of injuries. Interestingly, the *Maf*$^{+}$ subset of CCK neurons is composed of transient vesicular glutamate transporter 3 (tVGLUT3) neurons, which convey primarily dynamic allodynia. Identification of an etiology-based circuitry for mechanical allodynia in the dorsal horn has important implications for the mechanistic and clinical understanding of this condition.

INTRODUCTION

Mechanical allodynia is a highly prevalent persistent pain condition in which normally non-painful mechanosensory stimuli become painful after injury (Bouhassira et al., 2005). The key circuit-based transformations that give rise to mechanical allodynia occur within the spinal dorsal horn (Moehring et al., 2018; Todd, 2017; Peirs and Seal, 2016; Hughes and Todd, 2020), a major site for the integration of peripheral sensory information. This region is organized into six Rexed laminae, with the most superficial laminae (I and the outer part of II) responsible for processing acute pain, temperature, and itch and the deeper laminae (inner part of II–VI) important for innocuous touch and proprioception (Peirs and Seal, 2016; Gatto et al., 2019). Upon tissue and nerve damage stemming from a range of injuries broadly classified as neuropathic and inflammatory, mechanisms of disinhibition and sensitization are thought to make accessible a dorsally directed pathway that allows low-threshold mechanosensory afferents to activate more superficially located nociceptive circuits, thereby transforming touch into pain (mechanical allodynia) (Miraucourt et al., 2007; Torsney and MacDermott, 2006; Yasaka et al., 2014).

Excitatory populations important for conveying mechanical allodynia in the dorsal horn include those that belong to the somatostatin lineage, which forms a large heterogeneous population located throughout lamina II, at the lamina II/III border, in laminae I and deeper III, and including neurons that express calretinin (CR) and the gamma isoform of protein kinase C (PKCγ) (Chamessian et al., 2018; Peirs et al., 2020). Ablation of this population produced deficits in punctate (indentation with a von Frey filament, also known as static) and dynamic (light brushing across the skin surface) allodynia induced by both inflammatory and neuropathic injuries (Duan et al., 2014). In addition, significant deficits were noted in baseline von Frey threshold, pinprick, and paw pressure responses. The PKCγ-expressing neurons are located at the laminae II/III border and more sparsely in laminae I and deeper III. Based on manipulations of kinase activity, electrophysiological circuit mapping, and c-Fos analyses, this population of neurons is postulated to form the gate that allows low-threshold mechanosensory afferent recruitment of the dorsally directed nociceptive pathway after injury (Artola et al., 2020).

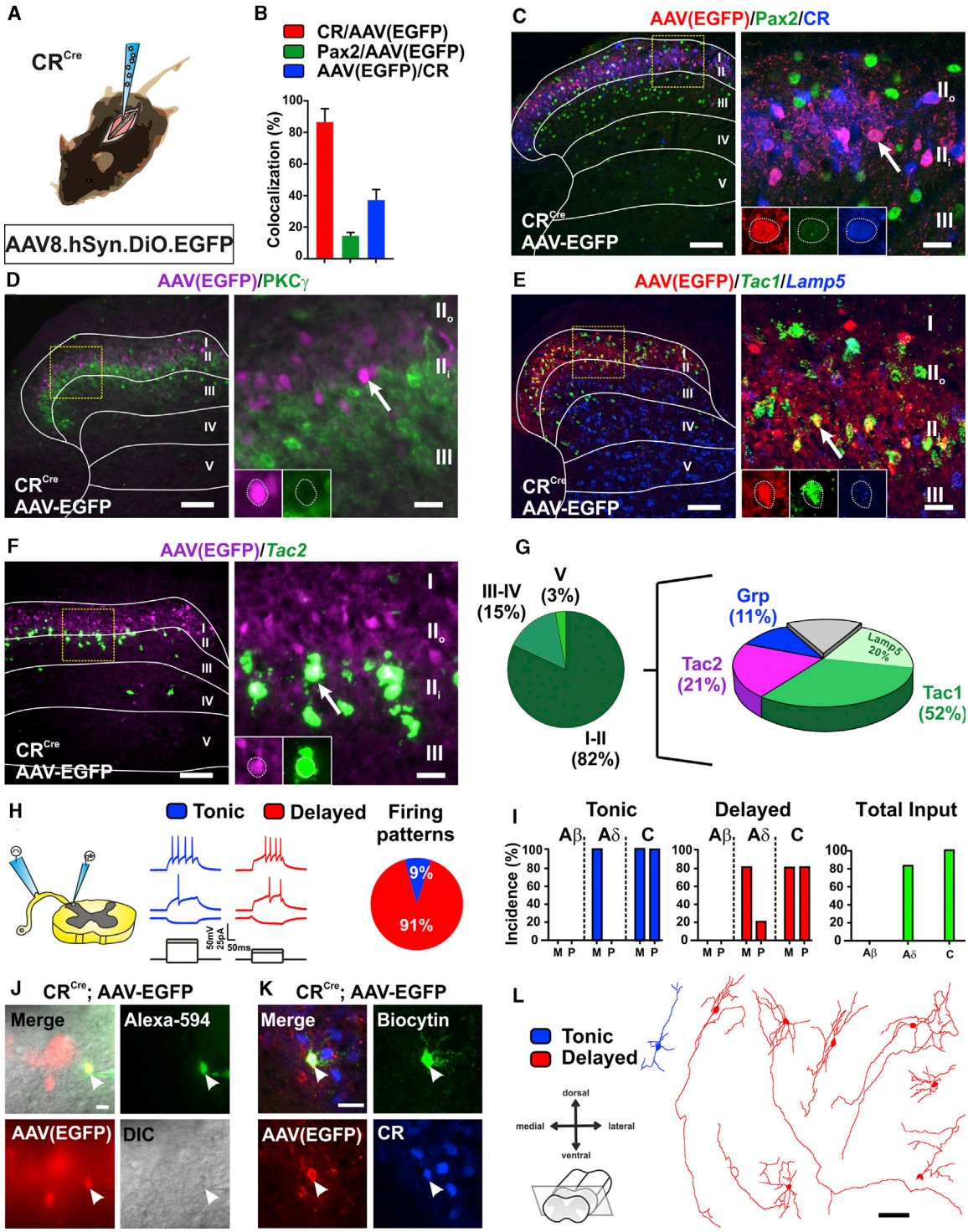

Figure 1. Molecular, Electrophysiological, and Morphological Characterization of Virally Targeted CR Neurons

(A) Schematic of CR^{Cre} mouse intraspinally injected with AAV8.hSyn.DIO.EGFP virus.

(B and C) Most virally targeted $EGFP^+$ neurons (red) express CR (blue), and a small number of those also express Pax2 (green). Data are mean ± SEM. The yellow box shows the location of the inset. Arrow shows CR and EGFP colocalized cell. Scale bars, 100 and 20 μm.

(D) $EGFP^+$ neurons (magenta) do not overlap (arrow) with PKCγ (green). The yellow box shows the location of the inset. The arrow points to an example of an $EGFP^+$ cell. Scale bars, 100 and 20 μm.

(legend continued on next page)

More recent studies have reported on populations of excitatory neurons located in the deeper dorsal horn (laminae III–V), referred to as the low-threshold mechanoreceptor (LTMR) recipient zone, that also overlap significantly with the PKCγ population, including cholecystokinin (CCK) neurons in laminae II–IV (Abraira et al., 2017; Gutierrez-Mecinas et al., 2019a). These neurons were recently shown to be important for mechanical allodynia and to receive facilitatory descending modulation from the cortex (Liu et al., 2018). Neurons in lamina II–IV that transiently express the vesicular glutamate transporter 3 during postnatal development (tVGLUT3) were also shown to have a role in mechanical allodynia (Peirs et al., 2015). VGLUT3 knockout (KO) animals exhibit deficits in both punctate and dynamic allodynia following neuropathic and inflammatory injuries, with no effect on baseline von Frey thresholds or response to light brush (Peirs et al., 2015; Seal et al., 2009). Ablation of tVGLUT3 neurons in adult mice produced slightly different phenotypes, a deficit in dynamic but not punctate mechanical allodynia in inflammatory and neuropathic pain models, and an increase in baseline von Frey threshold (Cheng et al., 2017).

Lastly, CR neurons in lamina II were identified as potentially having a role in mechanical allodynia based on the analysis of c-Fos following activation of the tVGLUT3 neurons with an excitatory designer receptor (eDREADD) (Peirs et al., 2015). Intriguingly, subsequent c-Fos analyses for mechanical allodynia performed in the context of persistent pain models showed a higher number of c-Fos$^+$ cells in CR neurons after inflammatory injury than after neuropathic injury, whereas the opposite pattern was observed in PKCγ neurons (Peirs et al., 2015). While it has been well established that mechanical allodynia is mediated by peripheral neural circuits that differ by injury type, these c-Fos experiments were the first to suggest that the circuitry in the dorsal horn also differs by the nature of the injury.

Here, we use pharmacological and virally introduced chemogenetic manipulations to probe the involvement of CR and PKCγ neurons in a large number of persistent pain models to determine whether participation of these neurons in the circuitry for mechanical allodynia differs by the type of injury. We also show that excitatory CCK neurons in lamina III–IV, distinct from the CR and PKCγ populations, are important for punctate and dynamic mechanical allodynia induced by both inflammatory and neuropathic injuries. Furthermore, we report that the tVGLUT3 population, required primarily for dynamic mechanical allodynia, is a subset of these CCK neurons. These findings provide a more comprehensive view of the dorsal horn mechanical allodynia circuitry and a framework for future studies to identify the mechanisms underlying the induction and maintenance of the allodynic state as a function of injury type. This new perspective is also important for the development and validation of persistent pain therapies that target this region, as preclinical and clinical studies point to the nature of the injury as a key factor in therapeutic effectiveness (Finnerup et al., 2015).

RESULTS

Characterization of Targeted Lamina II Calretinin Neurons

We previously reported that CR neurons in lamina II robustly upregulate c-Fos in response to low-threshold mechanical stimulation in the carrageenan model of inflammatory pain (Peirs et al., 2015). However, this population shows very little overlap with c-Fos in the spared nerve injury (SNI) model of neuropathic pain (Peirs et al., 2015), leading us to hypothesize that the CR neurons convey mechanical allodynia induced by inflammatory but not neuropathic injuries.

Here, we test this hypothesis using an inhibitory designer receptor approach that allows us to acutely inhibit the neurons while assessing pain behavior. A viral targeting strategy was used to express the designer receptor specifically in dorsal horn CR neurons. CR neurons represent a significant percentage of the excitatory neurons in laminae I–II (~42%) and can be divided into subpopulations that also express gastrin-related peptide (Grp), tachykinin 1 (Tac1), tachykinin 2 (Tac2), or PKCγ (Häring et al., 2018; Peirs et al., 2020). Fifteen percent of CR neurons in lamina II are inhibitory, with a significant proportion of those expressing Tac1 (Gutierrez-Mecinas et al., 2019b; Smith et al., 2015). To identify the particular subpopulation(s) of CR neurons captured by our viral targeting approach, we expressed soluble enhanced green fluorescent protein (EGFP) in the neurons by injecting AAV8.hSyn.DIO.EGFP in the dorsal horn of P21 CR^{Cre} mice (Figure 1A) and then performed *in situ* hybridization and immunohistochemistry. Importantly, viral expression was excluded from brain and dorsal root ganglion (DRG) neurons (data not shown), consistent with previous reports using similar viral vectors (Cui et al., 2016; Peirs et al., 2015). Nearly all EGFP$^+$ neurons expressed CR (~90%) (Figures 1B and 1C) and a small percentage of these (~14%) expressed Pax2, a marker of inhibitory neurons (Figures 1B and 1C). None of the targeted CR neurons expressed PKCγ (Figure 1D). *In situ* hybridization performed on the dorsal horns of injected mice with probes to the Tac1, Tac2, and Grp subpopulations showed that their degree of colocalization with the virally targeted population was in approximate proportion to their presence within the larger CR population (Figures 1E–1G) (Gutierrez-Mecinas et al., 2019b).

To further characterize this subset of virally targeted CR neurons, we performed patch clamp electrophysiological recordings on EGFP$^+$ cells in spinal cord slices with DRG still attached (Figure 1H). We assessed both action potential firing patterns in response to current injection and primary afferent input types (Figure 1I). Immunohistochemistry to identify the recorded cells

(E and G) Viral expression of EGFP (red) is largely contained within dorsal horn lamina II. Infected neurons overlap with *Tac1* (with and without *Lamp5*) (52%), *Tac2* (21%), and *Grp* (11%). The yellow box shows the location of the inset. The arrow points to an example of a colocalized cell. Scale bars, 100 and 20 μm.
(H and I) Patch clamp recording in transverse lumbar spinal cord slices with dorsal root and DRG still attached. Nearly all EGFP$^+$ neurons show a delayed firing pattern in response to the current injection. One shows tonic firing. Neurons receive monosynaptic Aδ and mono- and polysynaptic C-fiber input with no Aβ input (n = 11 cells, N = 4 mice). M, monosynaptic; P, polysynaptic.
(J and K) Recorded cells are filled with Alexa 594 and biocytin for post hoc reconstruction and to confirm EGFP and CR expression. Scale bars, 20 μm.
(L) Morphology of recorded cells in (H). Scale bar, 50 μm.

(Figures 1J and 1K) and to reconstruct dendritic morphologies (Figure 1L) was performed following the recordings. All but one of the EGFP$^+$ neurons (91%) showed a delayed firing pattern in response to current injection (Figure 1H), consistent with reports for the larger CR population (Smith et al., 2015). With respect to the types of primary afferent input, ~80% of the EGFP$^+$ neurons received Aδ input and all of them received C-fiber input (Figure 1I). Mono- and polysynaptic Aβ input onto the EGFP$^+$ neurons was never detected (Figure 1I). Dendritic morphologies of this subpopulation of CR neurons were diverse, including radial, vertical, and unknown types, again consistent with morphologies reported for the lineage-traced CR neurons (Figure 1L) (Smith et al., 2015). Interestingly, CR neurons show remarkably elongated arbors in the dorsoventral direction, suggesting synaptic connectivity that extends beyond lamina II (Figure 1L). This finding is supported by the relatively high incidence of both monosynaptic Aδ- and C-fiber inputs observed in patch clamp recordings compared to other populations of dorsal horn neurons (Cordero-Erausquin et al., 2016).

Role of Lamina II Calretinin Neurons in Mechanical Allodynia

For behavior experiments, we chose the designer receptor PSAM-GlyR, in which the ligand-binding domain of the human α7-nicotinic receptor is fused to the anion channel domain of the human glycine receptor. Mutations in the ligand-binding domain allow selective recognition of PSEM^{89S} (Magnus et al., 2011). To test the ability of PSAM-GlyR to inhibit dorsal horn excitatory neurons, we performed patch clamp electrophysiological recordings in spinal cord slices from Tlx3^{Cre} mice intraspinally injected with the AAV8.hSyn.FLEX.PSAM-GlyR (Figures S1A–S1E). The Tlx3^{Cre} line allowed us to test a range of excitatory populations. Bath application of PSEM^{89S} (30 μM) to spinal cord slices caused membrane potential hyperpolarization and completely blocked action potential firing due to the injection of depolarizing currents, only in neurons expressing PSAM-GlyR (Figures S1D and S1E).

To determine the role of the CR neurons in pain behavior, we injected AAV8.hSyn.FLEX.PSAM-GlyR virus unilaterally into the dorsal horn of P21 CR^{Cre} mice (Figure 2A). The distribution of the receptor in the dorsal horn was visualized with α-bungarotoxin-Alexa 647 (α-BTX-Alexa 647), which recognizes the ligand-binding domain of the α7-nicotinic receptor. Neurons expressing PSAM-GlyR were restricted to lamina II and co-localized with CR, but not PKCγ (Figure 2B), similar to EGFP in Figure 1 and to the excitatory designer receptor targeted to this population in a previous study (Peirs et al., 2015). No α-BTX-Alexa 647 staining was observed on the contralateral side of the spinal cord, indicating specificity of the reagent for PSAM-GlyR in dorsal horn tissue (Figures S1F and S1G). Importantly, as a control for the specificity of the ligand, we also show that the injection of PSEM^{89S} has no effect on persistent pain behavior induced by carrageenan, complete Freund's adjuvant (CFA), or SNI in mice lacking PSAM-GlyR (Figures S1H–S1J).

We first tested PSAM-GlyR-expressing CR^{Cre} mice in acute somatosensory behaviors by measuring von Frey thresholds, cotton swab responsiveness, pinprick response, response threshold to calibrated calipers (pressure), latency to remove a piece of sticky tape, and Hargreaves heat sensitivity both before and after injection of PSEM^{89S}. Inhibition of the targeted CR neurons had no effect on any baseline somatosensory behavior (Figures S2A and S2B). Performance on the rotarod was also unaffected (Figure S2B), indicating that the CR neurons are also dispensable for gross motor function.

Next, we determined whether the neurons are required for conveying mechanical allodynia induced by inflammatory injuries using several well-established pain models, starting with the carrageenan and more persistent CFA models. Mechanical sensitivity of the hindlimbs was assessed before injury, and then within the peak of the allodynic state, after induction and before resolution. Twenty-four hours after intraplantar injection of carrageenan, von Frey thresholds (punctate allodynia) were significantly decreased and responsiveness to a cotton swab (dynamic allodynia) was significantly increased (Figure S2C). Subsequent injection of PSEM^{89S} caused a significant increase in the von Frey thresholds but not a significant change in the responsiveness to a cotton swab (Figure S2C). Inhibition of CR neurons did not alter heat hypersensitivity in this model (Figure S2C). Measured 5–6 days after the injection of CFA into the plantar hind paw, systemic injection of PSEM^{89S} completely reversed punctate and dynamic mechanical allodynia induced by this model (Figure 2C).

To test whether the CR neurons are required for mechanical allodynia induced by neuropathic injuries, we used SNI models in which two of the three branches of the sciatic nerve are cut and ligated. Measured at 1, 2, and 6 weeks after sparing the sural nerve, the injection of PSEM^{89S} had no effect on either punctate or dynamic mechanical allodynia (Figures 2D and S2D). In the spared tibial model, which generates only punctate allodynia, the injection of PSEM^{89S} also had no effect (Figure S2E).

To further assess how generalizable the requirement for CR neurons is in the mechanical allodynia induced by inflammatory injuries, we tested an additional and highly clinically relevant model: the Brennan incision model of postsurgical pain, which, in contrast to the carrageenan and CFA models, does not focus on antigen-induced inflammation (Brennan et al., 2005). Inhibition of the CR neurons by intraperitoneal (i.p.) PSEM^{89S} injection in this model caused a statistically significant reversal of both punctate and dynamic mechanical allodynia (Figure 2E).

Lastly, we tested the role of the targeted CR population in chemically induced secondary mechanical allodynia models. Here, direct activation of peripheral nerve fibers at a primary site (ankle) leads to mechanical hypersensitivity at a secondary site (plantar surface) through central sensitization. Allodynia was induced by intradermal injection of 0.5% capsaicin or 10% mustard oil (allyl isothiocyanate [AITC]) proximal to the ankle. The former model relies on the activation of transient receptor potential cation channel subfamily V member 1 (TRPV1) (Caterina et al., 2000), whereas the latter model is induced by activation of the chemical irritant ion channel, TRPA1 (Bautista et al., 2006). Strikingly, inhibition of the CR neurons by i.p. PSEM^{89S} injection reversed mechanical allodynia induced by AITC, but not capsaicin (Figure 2F).

Intradermal injection of capsaicin is considered a model of neurogenic inflammation because it activates TRPV1-expressing fibers to cause the peripheral release of peptides that

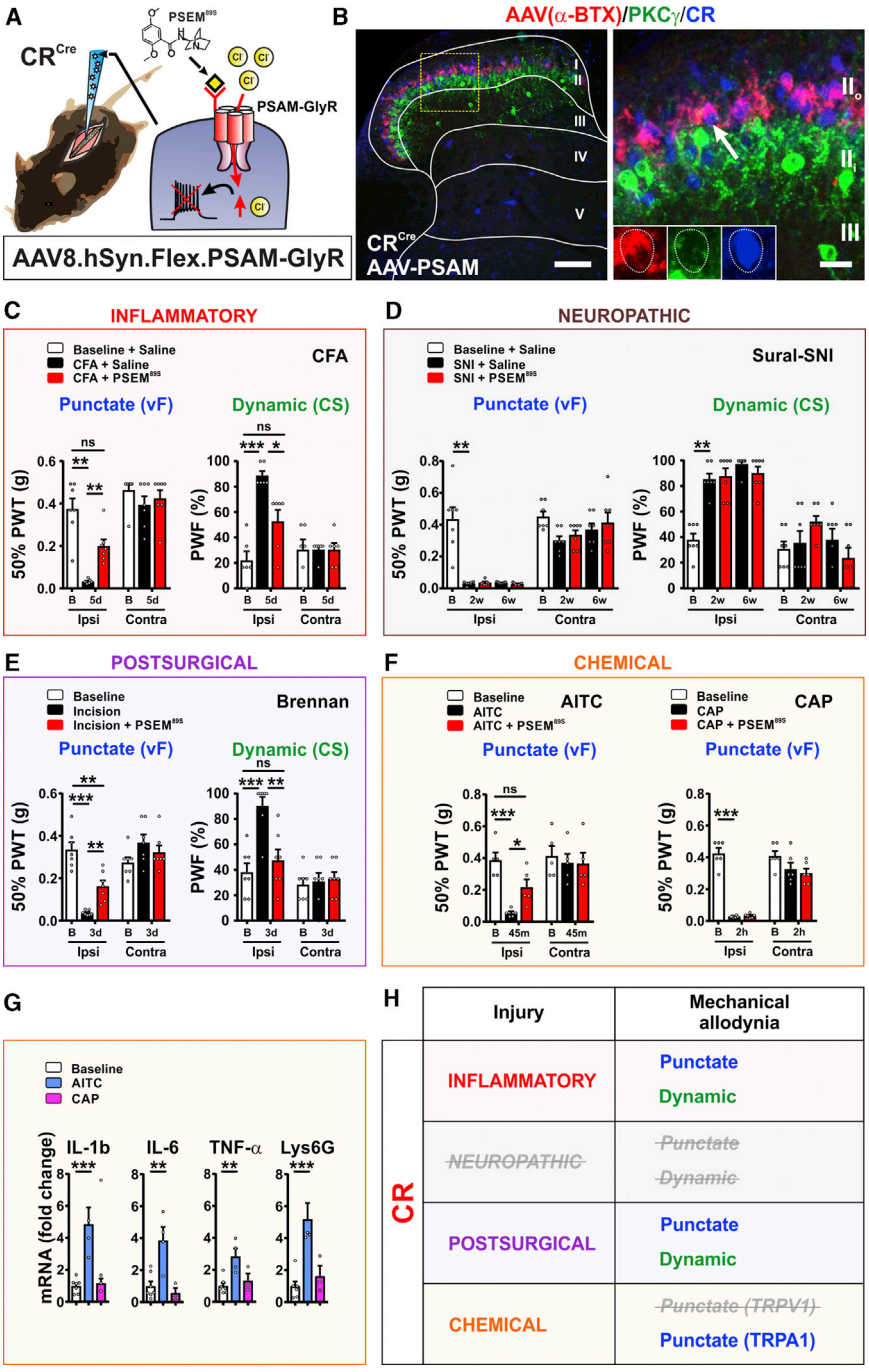

Figure 2. Targeted CR Neurons in Lamina II Are Important for Conveying Mechanical Allodynia Induced by Inflammatory but Not Neuropathic Pain Models

(A) Schematic of CR^{Cre} mice injected intraspinally with AAV8.hSyn.FLEX.PSAM-GlyR virus. PSEM^{89S} inhibits PSAM-GlyR-expressing cells.

(B) Dorsal horn shows α-BTX-Alexa 647 binding (red) to PSAM-GlyR is confined to lamina II. The receptor overlaps with CR (blue) but not PKCγ (green) neurons. The yellow box shows the location of the inset The arrow points to the colocalized cell. Scale bars, 100 and 20 μm.

(C) Mechanical allodynia induced by the CFA model is completely reversed by PSEM^{89S} (p = 0.0031, punctate; p = 0.0185, dynamic). N = 7 and 6 mice, respectively. PWT, paw withdrawal threshold; PWF, paw withdrawal frequency.

(D) PSEM^{89S} injection has no effect on mechanical allodynia at 2 and 6 weeks after sural SNI. N = 7 mice.

(E) In the postsurgical pain model, PSEM^{89S} injection partially reverses punctate allodynia and completely reverses dynamic allodynia (p = 0.0082, punctate; p = 0.0050, dynamic). N = 7 mice.

(F) Punctate mechanical allodynia after mustard oil (AITC) injection is reversed by PSEM^{89S} (p = 0.0485). N = 5 mice. Punctate allodynia induced by capsaicin (CAP) injection is unaffected by PSEM^{89S}. N = 6 mice.

(G) Levels of mRNAs for inflammatory mediators in the skin are increased after AITC but not CAP injection compared to vehicle injection. Skin was harvested immediately after allodynia measurements. N = 7 baseline, 4 AITC and 3 CAP mice.

(H) Summary of the role of targeted CR neurons in mechanical allodynia induced by persistent pain models.

Data are mean ± SEM. *p<0.05, **p<0.01, ***p<0.001. See also Figures S1 and S2.

promote vasodilation (flare) and subsequent inflammatory events (Matsuda et al., 2019). It was thus surprising that the inhibition of CR neurons had no effect on mechanical allodynia in this model. However, a previous study reported that the infiltration of neutrophils, a hallmark of inflammatory injury, does not occur with the intradermal injection of capsaicin in the secondary mechanical allodynia model until after the allodynia has resolved, raising questions about the inflammatory nature of this pain model (Sluka, 2002). We therefore tested whether other hallmarks of inflammatory injury, such as increased levels of the inflammatory mediators interleukin-6 (IL-6), interleukin-1β (IL-1β), tumor necrosis factor-alpha (TNF-α), and lymphocyte antigen 6 complex locus G6D (Lys6G), were present in the paw skin of the capsaicin-injected mice at the time of the allodynia. Mice were injected with AITC, which is known to induce an inflammatory response in this time frame, as a positive control, and with vehicle as a negative control. Harvested immediately after the allodynia measurement, AITC samples showed significantly higher levels of all four inflammatory mediators compared to vehicle (Figure 2G). In contrast, capsaicin samples showed the same level as vehicle. These results, together with the absence of edema and the report by Sluka (2002) on neutrophils, indicate that at the time of the allodynia, the capsaicin model lacked many hallmarks of an inflammatory injury. These results are thus consistent with the idea that CR neurons convey mechanical allodynia induced by inflammatory models.

Lastly, we show that the levels of *Calb2* in the dorsal horn are not altered by CFA injection (5 days) or SNI (7 days), indicating that the neuronal populations we inhibit in PSAM-GlyR-expressing CR^{Cre} mice do not change with injury (Figure S2F). Thus, behavioral data obtained from a number of pain models indicate that the virally targeted CR neurons in lamina II are important for conveying mechanical allodynia induced by inflammatory but not neuropathic injuries and are dispensable for capsaicin-induced secondary mechanical allodynia (Figure 2H).

Characterization of PKCγ Neurons in Mechanical Allodynia

In our previous study, we reported that c-Fos induction in the PKCγ population was greater when the mechanical allodynia was caused by SNI than by carrageenan injection, suggesting the participation of this population in conveying mechanical allodynia induced by neuropathic but not inflammatory injuries (Peirs et al., 2015). Original evidence pointing to the involvement of dorsal horn PKCγ neurons in mechanical allodynia came from studies of the kinase (Artola et al., 2020). Therefore, we examined whether the kinase itself has a role in the mechanical allodynia induced by neuropathic but not inflammatory injuries. For these experiments, we used both a potent and selective PKCγ inhibitor, tat-γV5-3, injected intrathecally (i.t.) (Sweitzer et al., 2004) as well as PKCγ KO animals (Abraira et al., 2017).

Histological analyses indicate that the PKCγ population is composed of three largely non-overlapping subpopulations defined by the expression of Tac2, neurotensin, and CCK (Peirs et al., 2020). We further characterized the neurons by assessing their electrophysiological properties and morphology in transverse spinal cord slices from mice expressing myristoylated GFP under the control of PKCγ regulatory elements ($PKC\gamma^{mGFP/+}$) (Figures 3A and 3B) (Abraira et al., 2017). Insertion of membrane-bound GFP (mGFP) at the start codon for PKCγ causes a loss of function. Nevertheless, heterozygous $PKC\gamma^{mGFP/+}$ mice, in contrast to PKCγ KO mice (Malmberg et al., 1997), show normal mechanical allodynia in a neuropathic pain model (Figure 3C). Myristoylated GFP^+ neurons in lamina II and at the lamina II/III border were targeted for recordings, and only neurons confirmed by post hoc staining to express PKCγ were included in the analyses (Figures 3D and 3E). Action potential firing patterns exhibited by the neurons in response to current injection were more diverse than what we observed with inner lamina II CR neurons, and included tonic (35.7%), phasic (28.6%), delayed (28.6%), and gap (7.1%) (Figure 3F). GFP^+ neurons received all types of afferent inputs, but the vast majority were from mono- and polysynaptic Aδ-fibers (Figure 3G). Consistent with a previous report (Abraira et al., 2017), minimal Aβ-fiber input was detected. Morphologies of the recorded cells were largely central and radial, with the exception of a few tonic cells that resembled vertical cells (Figure 3H), consistent with previous reports (Abraira et al., 2017; Alba-Delgado et al., 2015).

We next assessed the role of PKCγ in the acute somatosensory behaviors, sticky tape and pinprick, as well as in gross motor function on the rotarod using mice that lack PKCγ (homozygous $PKC\gamma^{mGFP/mGFP}$) (Figure 4A). The behavior of the mice in these assays was similar to WT littermates (Figure S3A). To assess whether PKCγ expression in the dorsal horn is required for conveying mechanical allodynia induced by models of inflammatory pain, we tested the mice 24 h after intraplantar injection of carrageenan and 5 days after intraplantar injection of CFA, to match the peak allodynic time points used to assess the involvement of CR neurons (Figures 2C and S2C). In both models, von Frey thresholds showed the same significant decrease as was observed with WT littermates (Figures 4B and S3B). Thermal hypersensitivity in the CFA model was also not affected by the loss of PKCγ (Figure S3B).

We then tested whether PKCγ conveys mechanical allodynia induced by neuropathic pain models. In both tibial and sural SNI models, von Frey thresholds measured 1 week after injury were significantly higher than those of the wild-type (WT) littermates (Figures 4C and S3C). These results are consistent with what was reported for PKCγ KO mice using the partial nerve ligation model of neuropathic pain (Malmberg et al., 1997) and confirm an important role for PKCγ in mechanical allodynia induced by neuropathy but not inflammation.

To further assess how generalizable the requirement for PKCγ neurons is in the mechanical allodynia induced by neuropathic but not inflammatory injuries, we also tested the mice using the Brennan incision model of postsurgical pain and the mustard oil (AITC) model of secondary mechanical allodynia. Similar to the other inflammatory pain models, the decrease in von Frey thresholds did not differ statistically between PKCγ KO mice and WT littermates (Figures 4D and 4E).

We next examined the role of local PKCγ in the dorsal horn using the specific and potent inhibitor tat-γV5-3 injected i.t. (Figure 4F). Similar to the KO, acute inhibition of PKCγ had no effect on the mechanical allodynia induced by intraplantar injection of carrageenan or CFA (Figures 4G and S3D), whereas i.t. injection of the PKCγ inhibitor 1 week after tibial SNI showed a partial reversal of the allodynia (Figure 4H), similar to a previous report (Petitjean et al., 2015). Acute inhibition of PKCγ also does not affect postsurgical mechanical allodynia (Figure 4I). Lastly, acute inhibition of PKCγ in the dorsal horn attenuates secondary mechanical allodynia induced by intradermal capsaicin (Figure 4J), consistent with a previous report (Petitjean et al., 2015). Together, the data demonstrate that the kinase itself is required for mechanical allodynia induced by neuropathic but not inflammatory injuries, as well as for capsaicin-induced secondary mechanical allodynia.

To determine whether PKCγ neurons have a role in mechanical allodynia induced by neuropathic but not inflammatory injuries, we expressed PSAM-GlyR in the lumbar dorsal horn of $PKC\gamma^{CreERT2}$ mice. Here, a tamoxifen-inducible Cre recombinase is expressed under the control of PKCγ regulatory elements, similar to the $PKC\gamma^{mGFP}$ mice (Abraira et al., 2017). We compared the distribution of Cre recombinase activity and endogenous PKCγ in the dorsal horn by crossing $PKC\gamma^{CreERT2}$ mice to Ai14-tdTomato reporter mice. Tamoxifen (1.5 mg, i.p.) was injected for 5 consecutive days starting at postnatal day 25 (P25) and the dorsal horn examined 2–3 weeks later. Ninety percent of $tdTomato^+$ neurons expressed the kinase and ~75% of $PKC\gamma^+$neurons expressed tdTomato (Figures S3E–S3G).

Surprisingly, adeno-associated viruses (AAVs) with human synapsin promoter do not show transgene expression in PKCγ

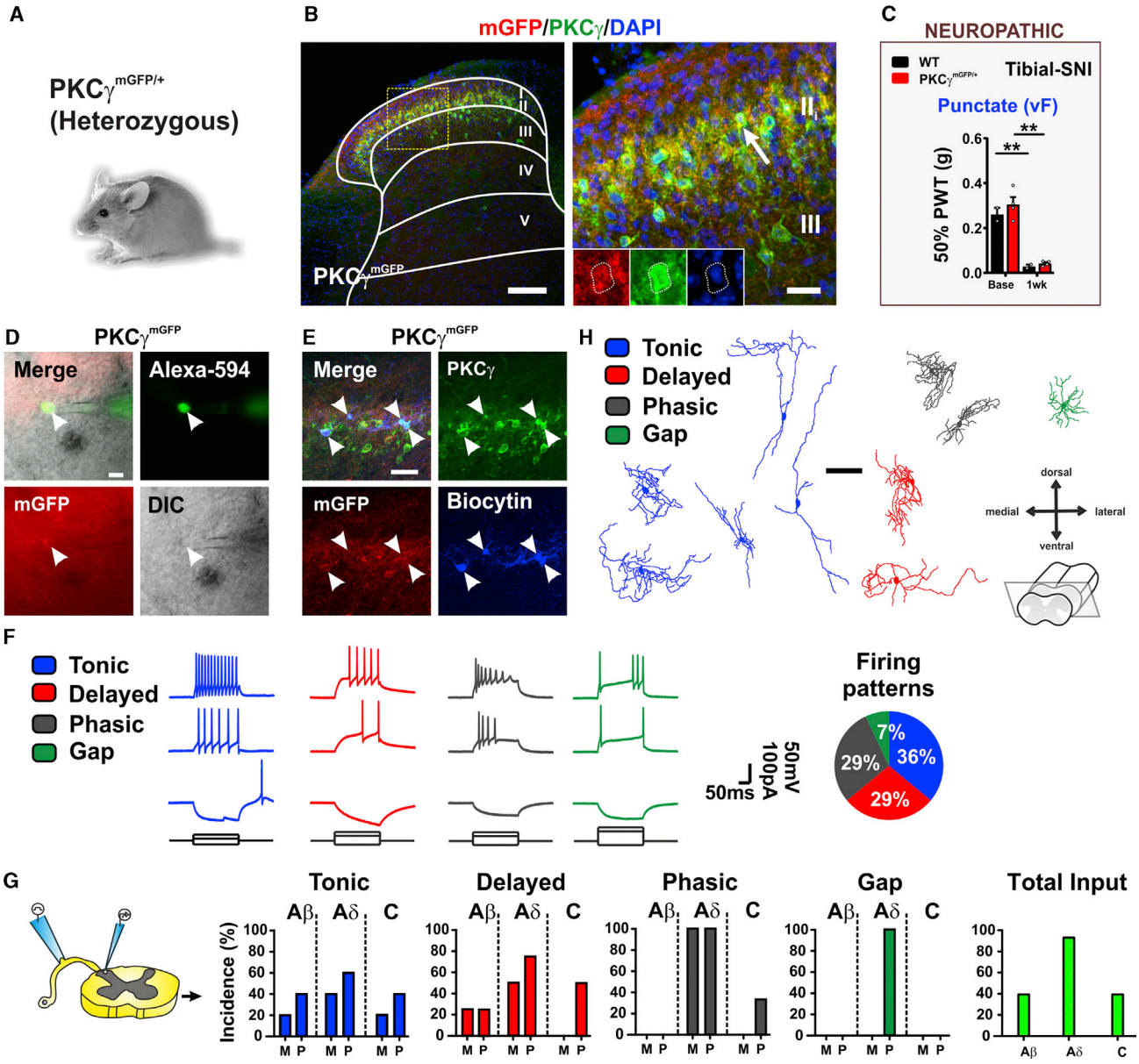

Figure 3. Electrophysiological and Morphological Characterization of PKCγ Interneurons

(A and B) Dorsal horn of adult mice heterozygous for myristoylated GFP knockin allele (PKCγ$^{mGFP/+}$) immunostained for mGFP (red), PKCγ (green), and DAPI (blue). GFP and PKCγ are co-expressed in lamina II (arrow). The yellow box shows the location of the inset. Scale bars, 100 and 20 μm.

(C) PKCγ$^{mGFP/+}$ mice develop punctate mechanical allodynia similar to WT littermates after tibial SNI. N = 2 WT and 4 PKCγ$^{mGFP/+}$ mice. Data are mean ± SEM. **p<0.01

(D and E) Patch clamp recording of mGFP^{+} cells in lamina II and II/III border in transverse spinal cord slices with dorsal root and DRG still attached. The recorded cells are filled with Alexa 594 and biocytin for post hoc reconstruction and to confirm mGFP (red) and PKCγ (green) expression. Scale bars, 20 μm.

(F and G) Firing patterns in response to current injection are tonic, delayed, or phasic with a few gaps. Tonic and delayed cells receive all input types, except that delay neurons do not show monosynaptic C-fiber input. Phasic firing cells receive largely Aδ and some C-input but no Aβ input. Gap firing cells receive only polysynaptic Aδ input (n = 14 cells, N = 6 mice). M, monosynaptic; P, polysynaptic.

(H) Morphology of the recorded cells in (F). Scale bar, 50 μm.

neurons. For example, EGFP and PKCγ do not overlap after the injection of AAV8.DIO.hSyn.EGFP into VGLUT2^{Cre} mice, which express Cre in PKCγ neurons (Figures S3H and S3I). We took advantage of this to exclude PKCγ neurons when testing the role of CR and tVGLUT3 populations in the above experiments and in our previous study (Peirs et al., 2015). To express PSAM-GlyR in PKCγ^{+} neurons, we switched to the CAG promotor from Ai14 tomato reporter mice. PKCγ^{CreERT2} mice were

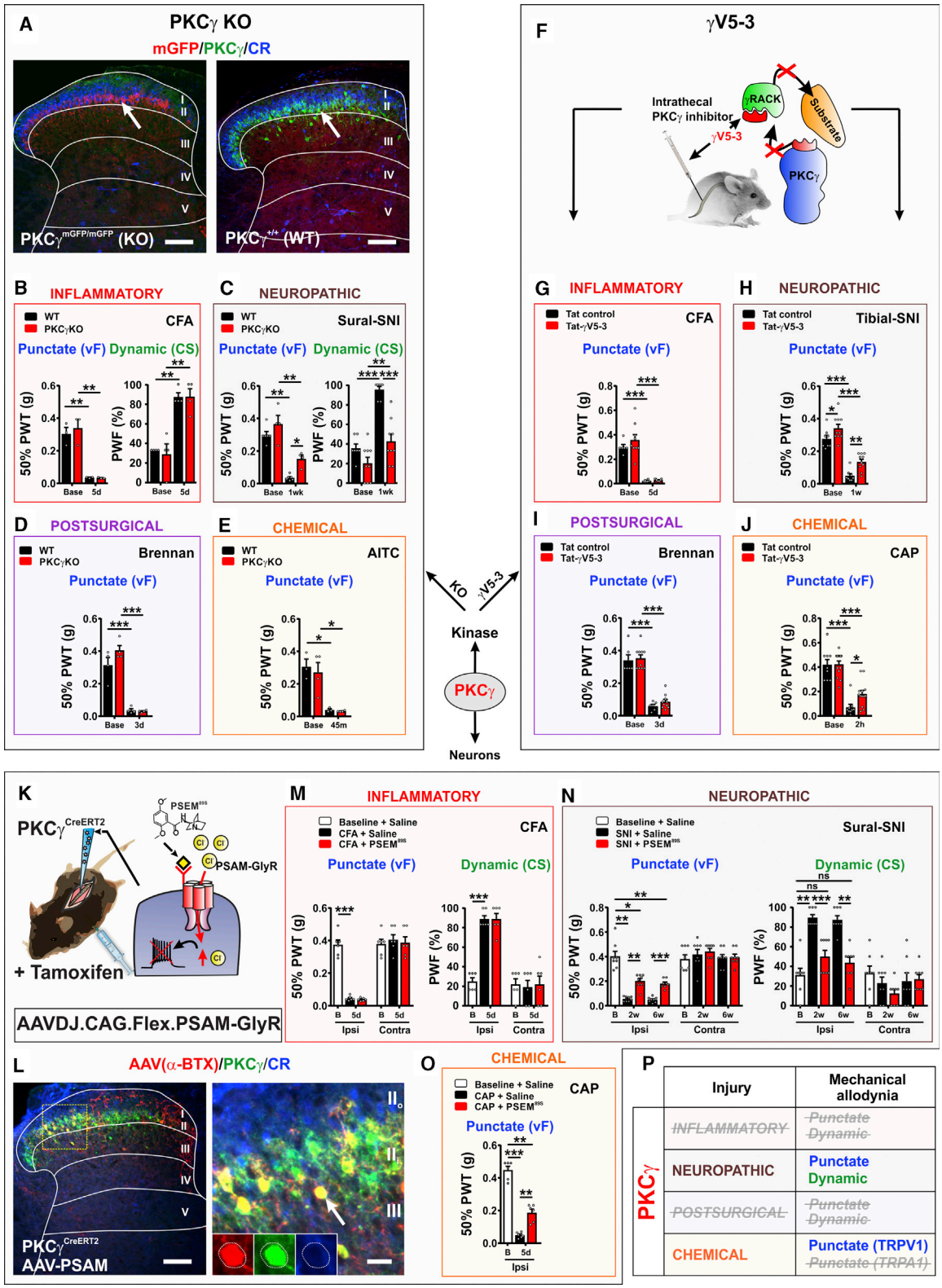

(legend on next page)

injected with AAVDJ.CAG.FLEX.PSAM-GlyR at P21 and then injected with tamoxifen (1.5 mg, i.p. for 5 days) (Figure 4K). PSAM-GlyR expression in PKCγ^{+} neurons was similar to what we observed with the tdTomato reporter mice (Figure 4L). As a side note, we used the DJ serotype, but AAV8 with the CAG promoter also shows expression in PKCγ neurons (data not shown).

We next used the mice to test acute and persistent pain behaviors. The injection of PSEM^{89S} had no effect on baseline behaviors (Figures S3J and S3K) or on von Frey thresholds or cotton swab responsiveness 5 days after intradermal CFA injection (Figure 4M). However, the injection of PSEM^{89S} significantly increased the von Frey thresholds and significantly decreased cotton swab responsiveness 1, 2, and 6 weeks after sural SNI (Figures 4N and S3L). The injection of PSEM^{89S} also partially reversed punctate mechanical allodynia induced by intradermal capsaicin (Figure 4O). The data therefore demonstrate for the first time that not only the kinase but also the PKCγ neurons themselves are important for conveying mechanical allodynia caused by neuropathic but not inflammatory injuries (Figure 4P).

Role of Deep Dorsal Horn Neurons in Mechanical Allodynia

Neurons that express CCK are present throughout the dorsal horn and are most concentrated in laminae II–IV. A recent single-cell sequencing study found that the neurons can generally be divided into three subpopulations (Maf, Cpne4, and Trh) based on the similarity of their gene expression profiles (Häring et al., 2018). The Trh subset also expresses PKCγ (Gutierrez-Mecinas et al., 2019a), raising the possibility that previous findings implicating CCK neurons in mechanical allodynia reflect the manipulation of these neurons (Liu et al., 2018). We therefore examined the role of CCK neurons that lacked PKCγ by using AAVs with human synapsin promoter driving the expression of the designer receptors (and EGFP reporter).

Viral targeting of AAV8.hSyn.DIO.EGFP in the dorsal horn of P21 CCK^{Cre} mice labeled neurons located primarily in the deep dorsal horn (laminae III–IV), that did not include CR or PKCγ expressing neurons (Figures 5A and 5B). As predicted, EGFP^{+} cells overlapped extensively with *Cck* and expressed *Cpne4* and/or *Maf*, but not *Trh* (Figures 5C–5F). We also characterized the electrophysiological properties and morphology of the targeted CCK neurons. Transverse spinal cord slices were prepared from P26–P30 CCK^{Cre} mice injected with AAV8.hSyn.DIO.EGFP at P16 (Figure 5G). Typical of deep dorsal horn neurons, the CCK neurons were either phasic (67%) or tonic (33%) firing (Figure 5H). Morphologies of the CCK neurons showed predominantly dorsoventral neurites (Figure 5I), resembling tVGLUT3 neurons in lamina III (Peirs et al., 2015).

To assess whether CCK neurons that do not include the PKCγ population have a role in pain, we used the excitatory designer receptor hM3Dq to activate the cells and measure behavior (Alexander et al., 2009). AAV8.hSyn.DIO.hM3Dq-mCherry was injected into the dorsal horn of P21 CCK^{Cre} mice. Three weeks later, the mice showed mCherry contained largely within laminae III–IV and not overlapping with CR or PKCγ (Figures S4A and S4B). The receptor also did not overlap with Pax2 (data not shown). Injection of the ligand, clozapine-n-oxide (CNO, 5 mg/kg i.p.) produced spontaneous behaviors (e.g., paw lifting, fluttering, guarding, licking, biting) and a statistically significant decrease in the von Frey threshold and increase in the cotton swab response frequency only at the ipsilateral hind paw (Figures S4C and S4D). These results suggested a role for the neurons in punctate and dynamic mechanical allodynia. Interestingly, unlike the targeted CR and tVGLUT3 populations (Peirs et al., 2015), activation of the

Figure 4. PKCγ and the Neurons that Express It Are Important for Conveying Mechanical Allodynia Induced by Neuropathic but Not Inflammatory Pain Models

(A) Mice homozygous for the mGFP knockin allele (PKCγ$^{mGFP/mGFP}$) express EGFP (red) but not the kinase (green) (PKCγ KO mice). Scale bar, 100 μm.

(B) Normal punctate and dynamic allodynia after CFA in PKCγ KO mice. N = 3–4 mice per genotype.

(C) Attenuation of punctate (p = 0.0138) and dynamic (p = 0.0001) mechanical allodynia induced by sural SNI in PKCγ KO (red bars) mice compared to WT littermates (black bars). N = 4–9 mice per genotype.

(D) Punctate allodynia induced by the postsurgical pain model does not differ between PKCγ KO and WT littermates. N = 4 mice per genotype.

(E) PKCγ KOs and WT littermates show similar punctate allodynia after mustard oil (AITC) injection. N = 3–4 mice per genotype.

(F) Schematic of intrathecal (i.t.) delivery of the PKCγ inhibitor, tat-γV5-3. The inhibitor prevents PKCγ from binding to the scaffolding protein RACK and its subsequent phosphorylation of substrates.

(G) Compared to the tat-control peptide (100 pmol) (black bars), injection of tat-γV5-3 (100 pmol) (red bars) has no effect on punctate mechanical allodynia induced by CFA. N = 9 tat-γV5-3, N = 6 tat control mice.

(H) i.t. injection of tat-γV5-3 (100 pmol) (red bars) partially reverses punctate mechanical allodynia (p = 0.008) induced by tibial-SNI (black bars). A small effect of tat-γV5-3 versus tat-control peptide at baseline is noted (p = 0.05). N = 10 tat-γV5-3, N = 8 tat control mice.

(I) i.t. injection of tat-γV5-3 (100 pmol) (red bars) has no effect on punctate mechanical allodynia (black bars) in the postsurgical pain model. N = 10 tat-γV5-3, N = 6 tat control mice.

(J) Injection of tat-γV5-3 (100 pmol) (red bars) but not the tat-control peptide (100 pmol) (black bars) partially reverses punctate allodynia (p = 0.0347) induced by capsaicin (CAP). N = 13 tat-γV5-3, N = 9 tat control mice.

(K) Schematic showing intraspinal injection of AAVDJ.CAG.FLEX.PSAM-GlyR virus into the PKCγ^{CreERT2} mice.

(L) Dorsal horn of PKCγ^{CreERT2} mice expressing PSAM-GlyR shows colocalization of α-BTX-Alexa 647 (red) with PKCγ (green) but not CR (blue). Scale bars, 100 and 20 μm.

(M) Injection of PSEM^{89S} has no effect on punctate or dynamic mechanical allodynia induced by CFA. N = 6 mice.

(N) Injection of PSEM^{89S} at 2 and 6 weeks after sural SNI partially reverses punctate (p = 0.0036, 2 weeks; p = 0.0002; 6 weeks) and fully reverses dynamic (p = 0.0009, 2 weeks; p = 0.0033, 6 weeks) allodynia. N = 7 mice.

(O) Punctate allodynia induced by CAP injected into the ankle is also partially reversed (p = 0.0051) by PSEM^{89S}. N = 6 mice.

(P) Summary of the role of PKCγ neurons in conveying mechanical allodynia induced by persistent pain models.

Data are mean ± SEM. *p<0.05, **p<0.01, ***p<0.001. See also Figure S3.

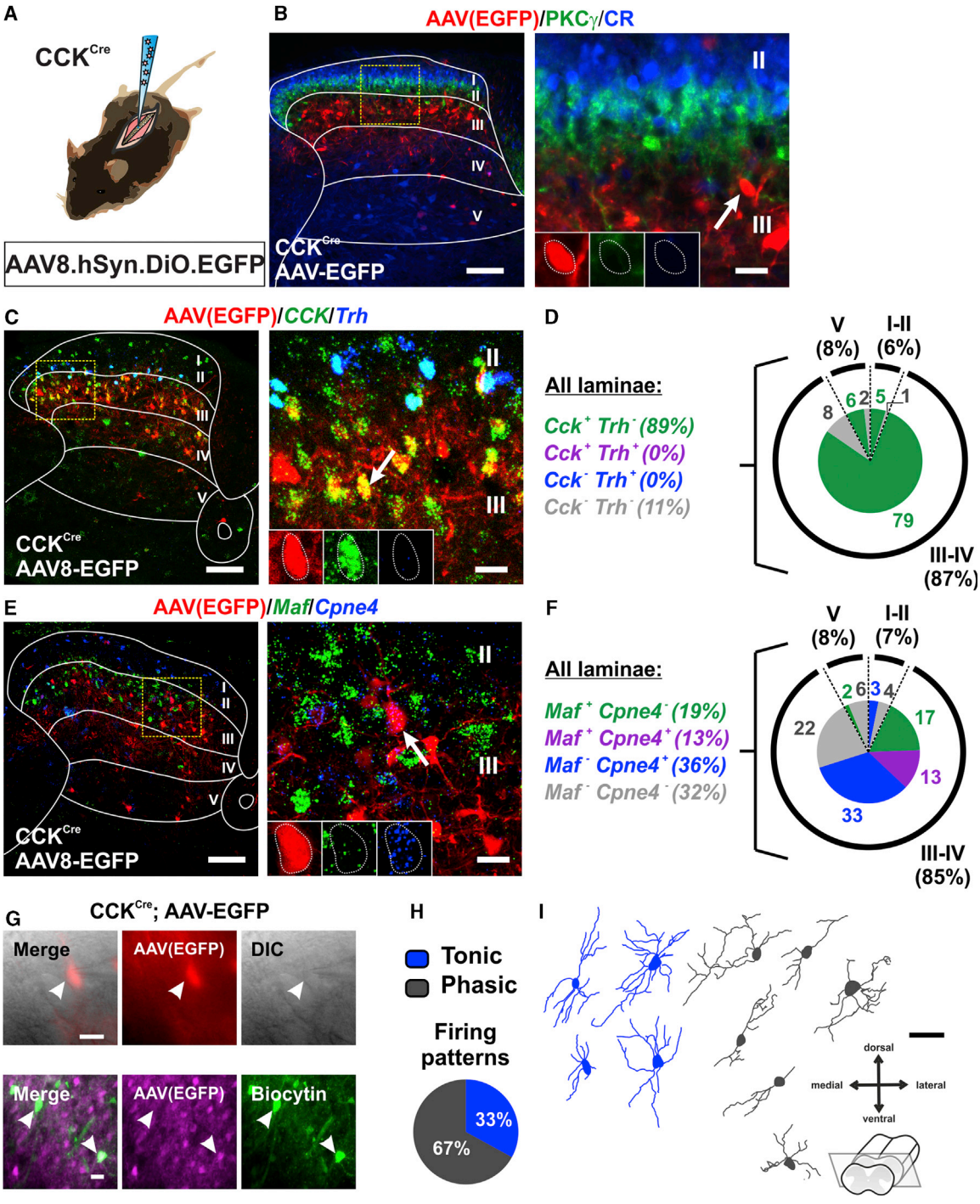

Figure 5. Molecular, Electrophysiological, and Morphological Characterization of Virally Targeted CCK Neurons

(A and B) Schematic of CCK^{Cre} mice injected with AAV8.hSyn.DIO.EGFP virus. In the dorsal horn, EGFP$^+$ neurons (red) are predominantly in lamina III with scattered cells in laminae II, IV, and V. Cells do not colocalize with PKCγ (green) or CR (blue). The yellow box shows the location of the inset. The arrow points to an example of an EGFP$^+$ cell. Scale bars, 100 and 20 μm.

(C and D) Nearly all EGFP$^+$ neurons (red) express *Cck* (green). Consistent with no PKCγ colocalization, none express *Trh* (blue). The values are percentages of the total EGFP$^+$ neurons. The yellow box shows the location of the inset. The arrow points to an example of a colocalized cell. Scale bars, 100 and 20 μm.

(E and F) Most EGFP$^+$ neurons (red) overlap with *Maf* (green) and/or *Cpne4* (blue). The values are a percentage of the total EGFP$^+$ neurons. The yellow box shows the location of the inset. The arrow points to an example of a colocalized cell. Scale bars, 100 and 20 μm.

(legend continued on next page)

CCK neurons also produced a statistically significant decrease in the paw withdrawal latency in the Hargreaves assay (Figure S4D), suggesting a role in heat hypersensitivity.

To determine whether the targeted CCK neurons are required for acute somatosensory or persistent pain behaviors, we injected AAV8.hSyn.FLEX.PSAM-GlyR unilaterally into the dorsal horn of P21 CCK^{Cre} mice (Figure 6A). Three weeks later, α-BTX-Alexa 647 staining showed a similar distribution for PSAM-GlyR as for the excitatory DREADD, including no colocalization with PKCγ, CR (Figure 6B), or Pax2 (data not shown). Tests of baseline somatosensory and motor behaviors showed only a statistically significant decrease in the latency to remove a piece of sticky tape from the ipsilateral plantar hind paw after the injection of PSEM^{89S} (Figures S4E and S4F).

In the inflammatory pain models, carrageenan, and CFA, injection of PSEM^{89S} caused a statistically significant decrease in both punctate and dynamic mechanical allodynia (Figures 6C and S4G). Heat hypersensitivity in the carrageenan model was also reversed after the injection of PSEM^{89S} (Figure S4G). One week after the induction of the SNI neuropathic pain models, the injection of PSEM^{89S} significantly attenuated both punctate and dynamic mechanical allodynia (Figures S4H and S4I). PSEM^{89S} injection similarly attenuated punctate and dynamic allodynia measured 2 and 6 weeks after sural SNI (Figure 6D). These data thus reveal for the first time a role for the PKCγ^{-} CCK neurons that reside largely in laminae III–IV in conveying mechanical allodynia induced by inflammatory and neuropathic pain models (Figure 6E).

The tVGLUT3-lineage neurons also reside in laminae II–IV and overlap with PKCγ (Cheng et al., 2017; Peirs et al., 2015). Ablation of the neurons in adult mice increased the baseline von Frey threshold and decreased dynamic but not punctate mechanical allodynia (Cheng et al., 2017). As with the CCK neurons, these observations also raised questions about the role of tVGLUT3 neurons that lack PKCγ. It also raised questions about how these neurons relate to CCK.

Thus, to assess the role of the tVGLUT3 population that excludes PKCγ neurons in pain behavior, we injected VGLUT3^{Cre} mice with the AAV8.hSyn.DIO.hM3Dq-mCherry virus. Since VGLUT3 is expressed transiently in the dorsal horn during postnatal development, peaking at ∼P9–P12 and disappearing by ∼P21, mice were injected from P7–P10 (Peirs et al., 2015). Examined 3 weeks later, the receptor was concentrated in laminae II–IV and did not colocalize with PKCγ (Figures S5A and S5B). We previously reported that activating these neurons with the excitatory DREADD produces spontaneous pain behaviors (guarding and fluttering) and punctate mechanical allodynia (Peirs et al., 2015). Here, we show that activating the neurons also produces dynamic mechanical allodynia (Figure S5C).

To test the requirement for this subset of tVGLUT3 neurons in acute somatosensory and persistent pain behaviors, we injected AAV8.hSyn.FLEX.PSAM-GlyR into the dorsal horn of VGLUT3^{Cre} mice at P7–P10 (Figure 7A). Staining with α-BTX-Alexa647 revealed a distribution of PSAM-GlyR resembling the excitatory DREADD, with labeled neurons located primarily in laminae III–IV and showing no overlap with CR or PKCγ (Figure 7B). The injection of PSEM^{89S} produced only a shorter latency in the sticky tape assay and had no effect on other acute behaviors or motor function (Figures S5D and S5E), similar to the inhibition of the CCK subset (Figures S4E and S4F).

In the persistent pain models, the injection of PSEM^{89S} completely reversed dynamic mechanical allodynia in both the carrageenan and sural SNI models, but only reversed punctate allodynia in the carrageenan model (Figures 7C and 7D and S5G). Carrageenan-induced heat hypersensitivity showed a minor reduction upon PSEM^{89S} injection that did not reach statistical significance (Figure S5F).

To determine the relationship between this subset of tVGLUT3 neurons and CCK, we injected AAV8.hSyn.DIO.EGFP into the dorsal horn of VGLUT3^{Cre} mice at P7–P10 and performed *in situ* hybridization 10–14 days later with probes to *Cck* and to the 3 markers (*Maf*, *Cpne4*, *and Trh*) of the CCK neuron clusters (GLUT1–3) defined by single-cell sequencing (Häring et al., 2018). The vast majority of EGFP^{+} neurons in lamina III–IV colocalized with *Cck* (81% = 59%/73%), and most of these neurons were *Maf*$^{+}$ (81% = 63%/78%) (Figures 7E–7H). Very few neurons were *Cpne4*$^{+}$ and none colocalized with *Trh*. In addition, to further characterize the tVGLUT3 subset, we assessed the colocalization of VGLUT3^{EGFP}-labeled neurons with the CCK-lineage neurons using CCK^{Cre} crossed to the Ai14-tdTomato reporter. In these mice at P12, 84% (346/411) of EGFP^{+} neurons overlapped with tdTomato (Figures 7I and 7J), indicating that the tVGLUT3 neurons are a nearly circumscribed subset of the CCK-lineage neurons important for dynamic mechanical allodynia induced by inflammation and nerve injury (Figure 7K).

DISCUSSION

Knowledge of the neural circuitry that conveys persistent pain is important for understanding underlying mechanisms and developing effective therapies. The work presented here focuses on the contribution of excitatory dorsal horn populations to the transmission of mechanical allodynia in the context of injury type. The data, together with studies that have probed the contributions of inhibitory interneuron populations (Peirs et al., 2020; Hughes and Todd, 2020), provide strong evidence for a model of the circuitry as a network of neural components differentially recruited, depending on the type of injury. Our revised model posits that with injury, multiple local circuits within the network allow low-threshold mechanosensory fibers to access nociceptive neurons through distinct mechanisms that are engaged according to the nature of the injury. Our findings substantially revise current models for the mechanical allodynia circuitry, which broadly describe a polysynaptic nociceptive pathway commonly activated regardless of injury type (Duan et al., 2014; Lu et al., 2013; Torsney and MacDermott, 2006; Yasaka et al., 2014). Our study thus provides a critical foundation for

(G) Patch clamp recordings (EGFP^{+}, red or magenta) in transverse slices of lumbar dorsal horn under differential interference contrast (DIC) and filled with biocytin (green). Scale bars, 20 μm.
(H) Firing patterns in response to current injection were tonic (67%) and phasic (33%). n = 20 cells, N = 6 mice.
(I) Morphology of neurons recorded in (H). Scale bar, 50 μm.

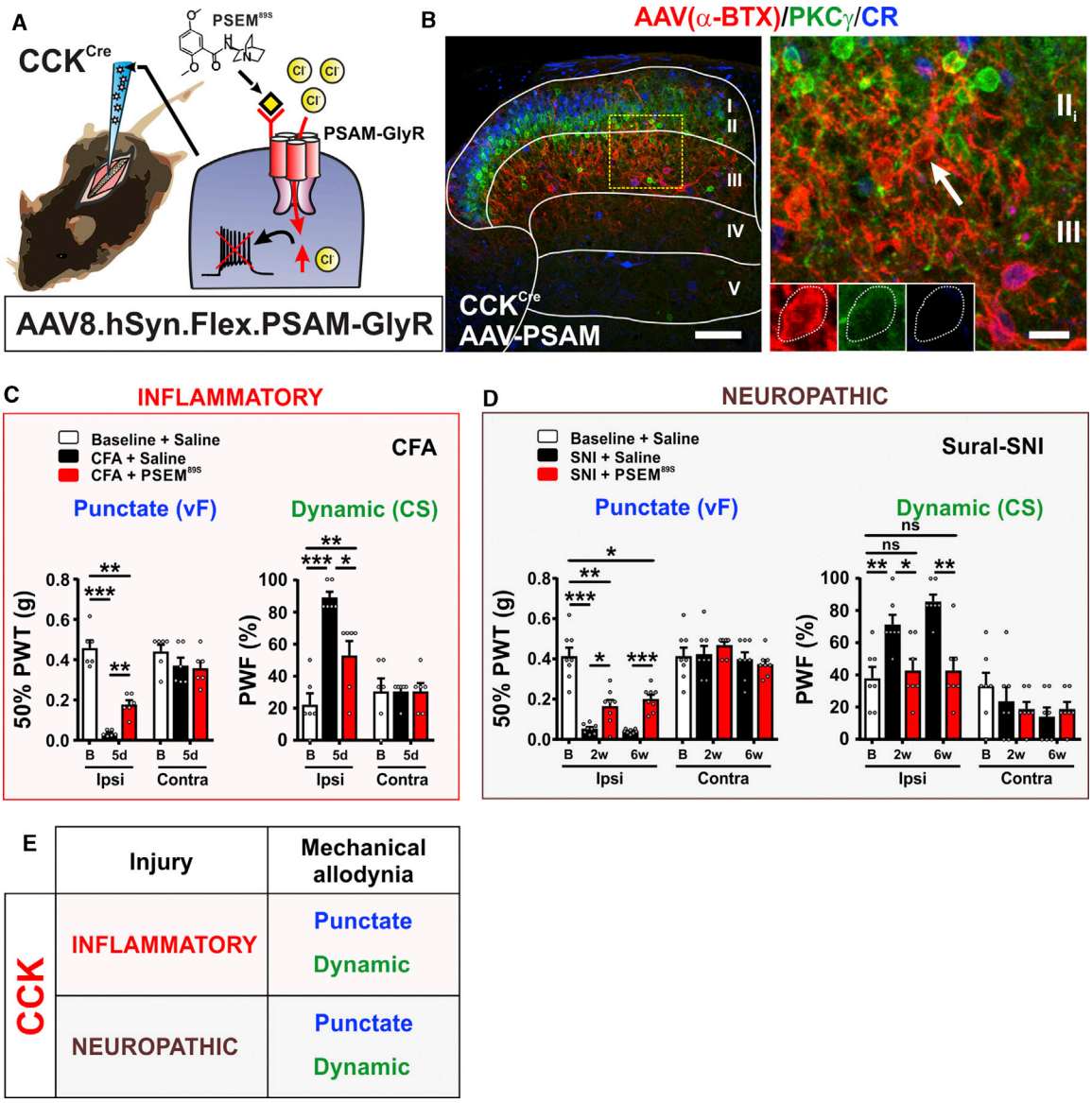

Figure 6. Targeted CCK Neurons Convey Mechanical Allodynia Induced by Both Inflammatory and Neuropathic Pain Models

(A and B) Schematic of CCK^{Cre} mice injected with AAV8.hSyn.FLEX.PSAM-GlyR virus. The dorsal horn shows α-BTX-Alexa 647 binding (red) in lamina III with scattered cells in laminae II, IV, and V. No overlap with PKCγ (green) or CR (blue) in laminae II or III. The yellow box shows the location of the inset. The arrow points to an example of a non-colocalized cell. Scale bars, 100 and 20 μm.

(C) PSEM^{89S} injection in CFA model partially reverses punctate ($p = 0.0051$) and dynamic ($p = 0.0185$) allodynia. N = 6 mice.

(D) PSEM^{89S} injection at 2 and 6 weeks after sural SNI partially reverses punctate ($p = 0.0264$, 2 weeks; $p = 0.0003$, 6 weeks) and completely reverses dynamic ($p = 0.0155$, 2 weeks; $p = 0.0022$, 6 weeks) allodynia. N = 7 mice.

(E) Summary of the role of targeted CCK neurons in conveying mechanical allodynia in persistent pain models.

Data are mean ± SEM. *p<0.05, **p<0.01, ***p<0.001. See also Figure S4.

future investigations into the mechanisms and local circuits that underlie the differential recruitment and maintenance of the network in the context of injury type.

For this study, we took advantage of expression profiles conferred by different AAV constructs and transgenic mouse lines to gain access to selective subpopulations of excitatory neurons. CR neurons within the inner part of lamina II, dorsal to the lamina II/III border, where the majority of PKCγ neurons reside, were specifically targeted, as were overlapping CCK and tVGLUT3 populations that reside ventral to the PKCγ layer in lamina III, and sparsely in laminae II, IV, and V. We also targeted the PKCγ neurons themselves. Although PKCγ neurons overlap with the larger CR, CCK, and tVGLUT3 populations, we avoided targeting those particular neurons when testing the latter populations by using AAVs that rely on the human synapsin promoter to drive the expression of the transgenes. This

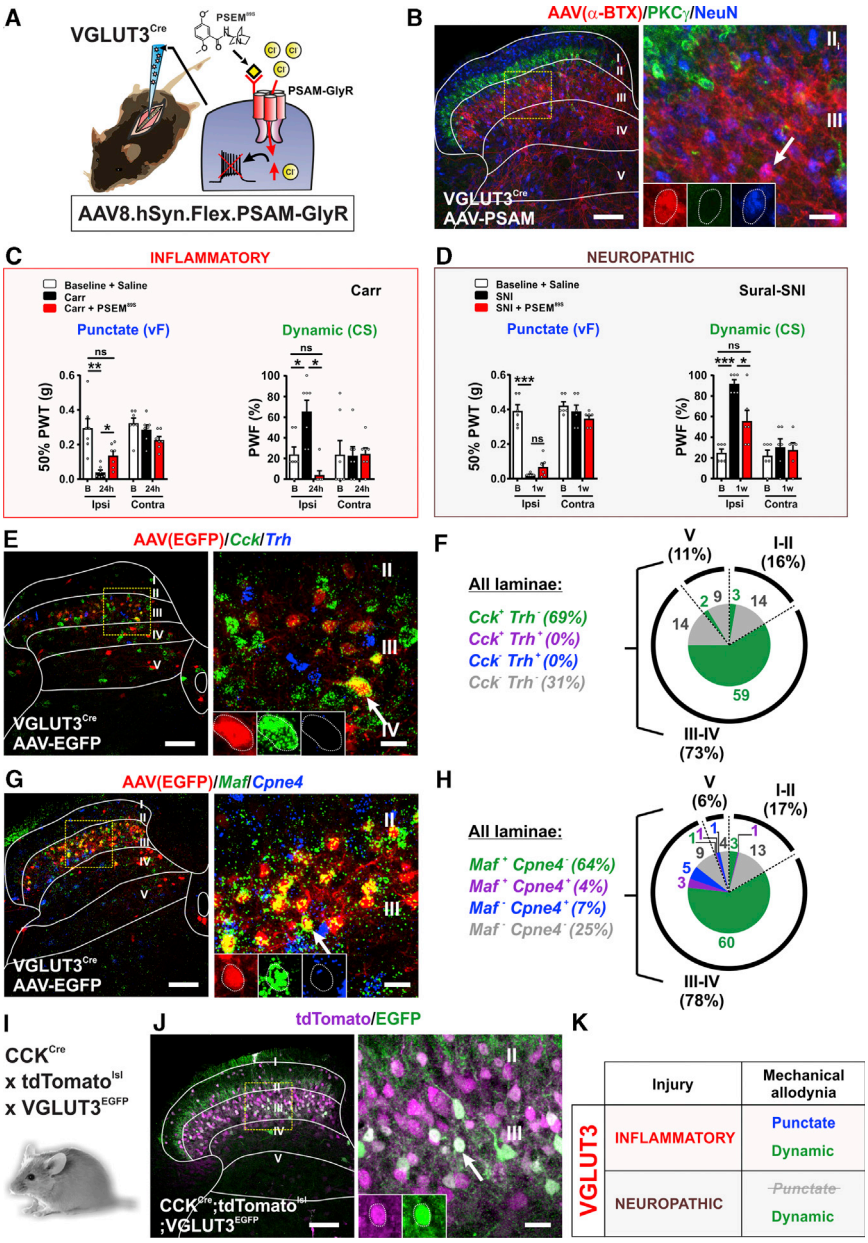

Figure 7. Role of Targeted VGLUT3 Neurons in Conveying Mechanical Allodynia Induced by Inflammatory and Neuropathic Pain Models

(A and B) Schematic of AAV8.hSyn.FLEX.PSAM-GlyR virus injected into VGLUT3^{Cre} mice. Staining with α-BTX-Alexa 647 (red) shows expression in lamina III with scattered cells in laminae II, IV, and V. The α-BTX-Alexa 647 (red) does not overlap with PKCγ (green). The yellow box shows the location of the inset. The arrow points to an example of an α-BTX-Alexa 647 (PSAM-GlyR)$^+$ cell. Scale bars, 100 and 20 μm.

(C) PSEM^{89S} injection reverses punctate ($p = 0.0109$) and dynamic ($p = 0.0126$) allodynia in the carrageenan model. N = 7 mice.

(D) PSEM^{89S} does not reverse punctate allodynia, but markedly reverses dynamic allodynia ($p = 0.0188$) in the sural SNI model. N = 6 mice.

(E and F) Dorsal horns from VGLUT3^{Cre} mice injected with AAV8.hSyn.DIO.EGFP show EGFP$^+$ neurons (red) primarily in dorsal horn laminae III–IV, where most overlap with *Cck* (green). Fewer EGFP cells express *Cck* in laminae II and V. No EGFP$^+$ neurons overlap with *Trh* (blue). The values are a percentage of the total EGFP$^+$ neurons. The yellow box shows the location of the inset. The arrow points to an example of a colocalized cell. Scale bars, 100 and 20 μm.

(G and H) EGFP$^+$ neurons (red) overlap with only *Maf* (red) (64%). Few express only *Cpne4* (blue) (7%) or both *Maf* and *Cpne4* (4%). The yellow box shows the location of the inset. The arrow points to an example of a colocalized cell. Scale bars, 100 and 20 μm.

(I and J) VGLUT3^{EGFP} BAC transgenic crossed to CCK^{Cre};Ai14-tdTomato mice show both reporters reside in lamina III with scattered cells in laminae II, IV, and V. Most EGFP$^+$ neurons (84%) express tdTomato. The yellow box shows the location of the inset. The arrow points to an example of a colocalized cell. Scale bars, 100 and 20 μm.

(K) Summary of the role of targeted tVGLUT3 neurons in conveying mechanical allodynia induced by persistent pain models.

Data are mean ± SEM. *p<0.05, **p<0.01, ***p<0.001. See also Figure S5.

promoter is generally assumed to be ubiquitously active in neurons. However, access to the PKCγ neurons required switching to the CAG promoter (i.e., in the PKCγ^{CreERT2} mice). Taking advantage of this promoter bias, we were able to investigate the molecular, morphological, and electrophysiological properties, as well as the functional roles of non-overlapping subpopulations of CR, PKCγ, and CCK/tVGLUT3 neurons.

Calretinin Neurons Convey Mechanical Allodynia in Inflammatory Injuries

We now show that targeted CR neurons in lamina II are important for conveying mechanical allodynia in pain models with a strong inflammatory component and not in neuropathic pain models. A previous study of CR-lineage neurons in the dorsal horn showed that conditional ablation of the neurons had no effect on punctate or dynamic allodynia in the sural SNI model, consistent with data reported here. Inflammatory models were not tested (Duan et al., 2014). Similar to what has been reported for the larger CR population, the targeted CR neurons express *Tac1*, *Tac2*, or *Grp*. A few also express Pax2. More important, the PKCγ subset was not captured. Tac1 interneurons (~73% express CR) have not been studied for a role in mechanical allodynia. Conditional ablation of the Tac2-lineage neurons (84% express CR) showed that they are dispensable for mechanical allodynia in the sural SNI model, but again, information about inflammatory models was not provided (Duan et al., 2014). Finally, the Grp (~55% express CR) population, which is known to be important for itch, has not been studied in models of persistent

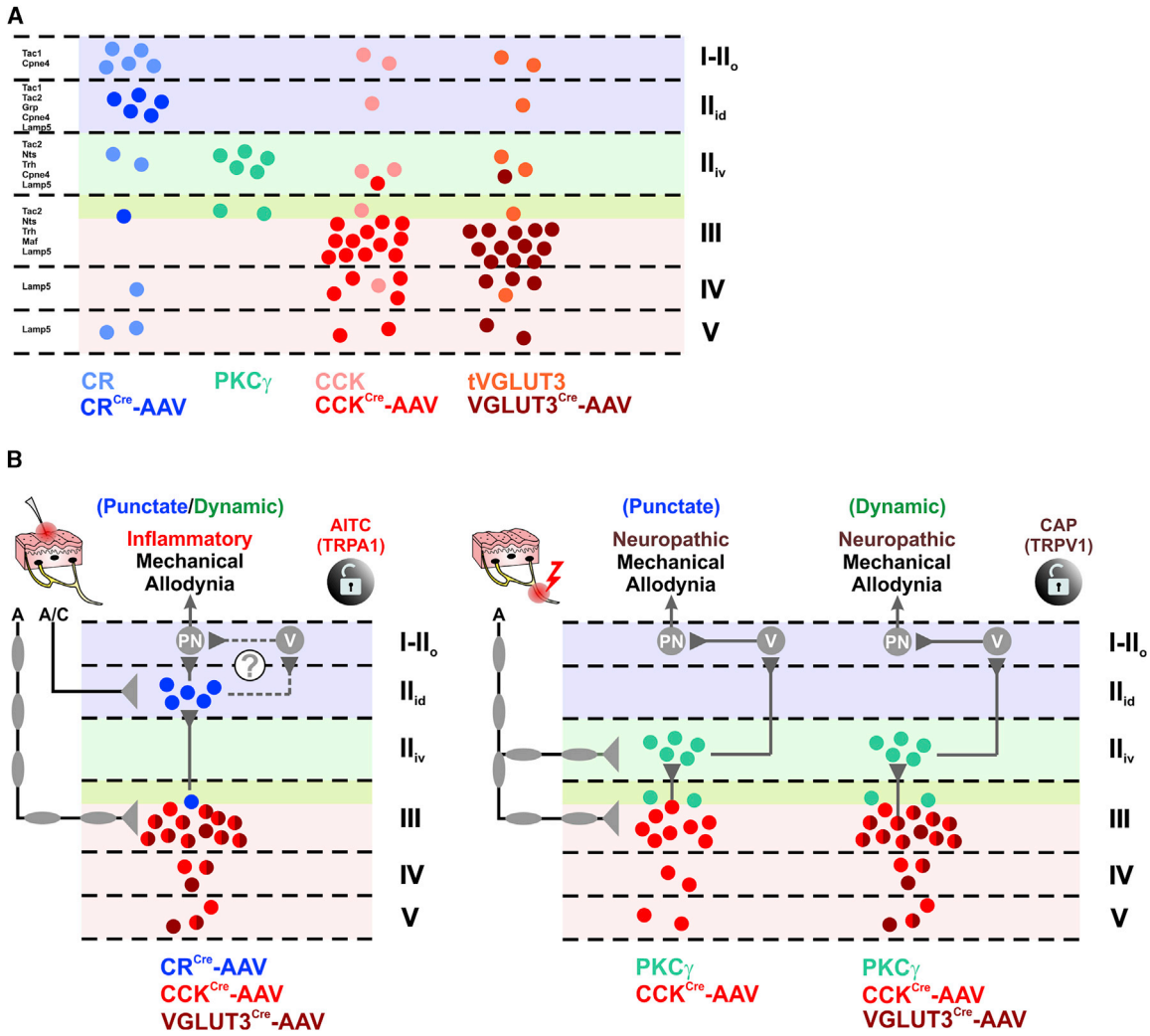

Figure 8. Dorsal Horn Circuitry Underlying Mechanical Allodynia Depends on the Injury Type

(A) Schematic of the laminar distribution of virally targeted (AAV) and lineage-derived populations discussed in this study. Virally targeted CR neurons (dark blue) are mostly restricted to the dorsal-inner part of lamina II (II$_{id}$) and largely exclude other CR-lineage neurons (light blue) in lamina I, the deep layers, and those expressing PKCγ. Nearly all of the PKCγ neurons were targeted by the virus (light green). Virally targeted CCK neurons (dark red) are highly concentrated in lamina III with scattered cells in laminae IV–V and generally exclude CCK-lineage neurons in the superficial laminae, including those expressing PKCγ (light red). Virally targeted tVGLUT3 neurons (dark brown) are highly concentrated in lamina III with scattered cells in laminae IV–V and generally exclude tVGLUT3-lineage neurons in superficial laminae, particularly those expressing PKCγ (light brown).

(B) Schematic diagram of the mechanical allodynia circuitry in the context of injury. Targeted CR neurons receive A- and C-fiber input, whereas targeted CCK/tVGLUT3 neurons receive predominantly A-fiber input. Left circuit: after inflammation, punctate or dynamic mechanical allodynia engage neurons expressing CCK/tVGLUT3 in lamina III, which activate the targeted CR neurons in lamina II$_{id}$. These CR neurons ultimately activate projection neurons (PNs) directly, or potentially indirectly through vertical cells, to elicit mechanical allodynia. A similar circuit is observed after activating TRPA1 through the peripheral injection of mustard oil (AITC). Right circuit: after nerve injury, punctate mechanical allodynia engages CCK, but not tVGLUT3 neurons in lamina III. These neurons then activate PKCγ neurons in lamina II$_{iv}$ and ultimately PNs indirectly through vertical cells. A similar circuit is observed for dynamic mechanical allodynia, but it also includes targeted CCK/tVGLUT3 neurons in lamina III. Mechanical allodynia induced by peripheral injection of the TRPV1 agonist capsaicin (CAP) also relies on PKCγ and CCK neurons.

pain. Although it is possible that the phenotype requires multiple subpopulations, probing each subpopulation individually may identify more specifically the relevant subset of CR neurons.

Inhibition of the targeted CR neurons showed no effect on baseline behaviors. In contrast, conditional ablation of the CR-lineage neurons led to an increase in the von Frey threshold and an increase in the latency to respond to a 54°C hotplate (Duan et al., 2014). CR-lineage neurons receive significant input from putative nociceptive C-fibers, including direct input from TRPV1$^+$ sensory afferents, and they also respond to pinch and capsaicin (Smith et al., 2015). The lack of baseline phenotypes observed in our study may be due to the composition of our targeted CR neurons. First,

the majority of targeted CR neurons were located in lamina II_i, just above PKCγ neurons, while the CR-lineage population also includes more dorsally located neurons, including those responding to noxious stimuli (Smith et al., 2015). Second, ablation of Tac1-lineage neurons, which also include a subset of lamina I projection neurons (PNs), did not produce deficits in nociceptive reflexes, but rather in "sustained" pain (Huang et al., 2019). Interestingly, Tac1-ablated mice showed deficits in sustained pain induced by intraplantar mustard oil but not capsaicin, similar to what we observed when inhibiting the CR-targeted neurons in secondary mechanical allodynia models. Ablation of Tac2-lineage neurons reportedly had no effect on acute somatosensory behavior (Duan et al., 2014). Finally, Grp neurons make up a small subset of the targeted CR neurons and respond primarily to pruritogens (Bell et al., 2020; Pagani et al., 2019; Sun et al., 2017). Although not exhaustively tested, these observations are consistent with the idea that the execution of acute somatosensory reflexes requires excitatory modules spanning a larger laminar area (see the accompanying paper by Gatto et al., 2020 in this issue of *Neuron*).

Interestingly, CR neurons are highly interconnected (Peirs et al., 2015; Smith et al., 2019) and poised to participate in a persistent pain network based on intrinsic and extrinsic properties that allow them to produce sustained activation following intense stimulation, and in this way act as a pain amplifier (Smith et al., 2019). Reflecting the larger population, targeted CR neurons receive predominantly C- and Aδ-fiber inputs, both of which have been implicated in the maintenance of CFA-induced mechanical allodynia (Lennertz et al., 2012; Singhmar et al., 2016). In rodents, peptidergic C-fibers labeled by calcitonin gene-related peptide (CGRP) densely innervate the outer part of lamina II, while non-peptidergic C-fibers send dense projections to the inner part of lamina II, where most of the CR neurons that we manipulate in our study reside. Conditional ablation of the non-peptidergic neurons abolished mechanical allodynia induced by CFA (Cavanaugh et al., 2009), while acute optogenetic inhibition of the more dorsally located CGRP afferents had no effect on mechanical allodynia induced by the Brennan incision model (Cowie et al., 2018). Correspondingly, non-peptidergic C-fibers express a very high level of TRPA1 but not TRPV1, whereas CGRP neurons express a very low level of TRPA1 but a high level of TRPV1 (Usoskin et al., 2015). Whether the CR neurons that we manipulate in this study receive synapses predominantly from non-peptidergic C-fibers remains to be determined.

PKCγ Neurons Convey Neuropathic Injury-Induced Mechanical Allodynia

Our work demonstrates a role for PKCγ neurons in conveying punctate and dynamic allodynia after neuropathic injury, consistent with observations obtained from indirect methods (Artola et al., 2020; Peirs et al., 2020). More important, we show that the neurons are not required for conveying allodynia induced by inflammatory injuries. We also show that there is a close correspondence between the requirement of the kinase and the neurons in the context of mechanical allodynia. Several studies have reported an increase in PKCγ expression in animal models of not only neuropathic but also inflammatory injuries (Artola et al., 2020). In our study, we observed an increase in dorsal horn *prkcg* mRNA in both the SNI and CFA models at the time of the allodynia measurement (Figure S2F). Interestingly, neuronal activity, revealed by the phosphorylation of ERK or c-Fos induction, can be detected in PKCγ neurons after mechanical stimulation of the skin in the first hours following the induction of inflammation (Alba-Delgado et al., 2018) but not 24 h or 2 days after the injection of carrageenan or CFA, respectively (Gao and Ji, 2010; Peirs et al., 2015). In contrast, neural activity is still detected in PKCγ neurons long after SNI induction (Peirs et al., 2015), suggesting that PKCγ neurons may play a role in the induction of both types of mechanical allodynia, but only in the maintenance of neuropathic mechanical allodynia. Interestingly, it was previously shown that under basal conditions, the kinase is already located predominantly at the cell membrane, in inactive peri-synaptic clusters apart from the synaptic cleft, which is a unique feature of spinal PKCγ compared to other brain areas (Peirs et al., 2014). A primary role for the kinase in the induction of the allodynic state in both models is also consistent with its suggested role in synaptic reinforcement through membrane receptor trafficking, and NMDA-dependent plasticity (Groc et al., 2004). Why long-term potentiation no longer requires PKCγ after induction of an inflammatory but not neuropathic injury remains to be determined. Nevertheless, these observations point to important differences that may underlie the maintenance of inflammatory versus neuropathic pain.

PKCγ neurons express Tac2 (~29%), neurotensin (~31%), or CCK (~47%) (Peirs et al., 2020). Negative results from conditional ablation of the Tac2-lineage neurons in neuropathic pain models (Duan et al., 2014) point to either the neurotensin or CCK subpopulations as having a role in mechanical allodynia. Nearly all neurotensin neurons express PKCγ (90%); however, information about a role for these specific neurons in persistent pain behaviors is lacking. With respect to the CCK subset of PKCγ neurons, these were excluded from our targeted CCK population and thus also remain a viable option.

Neurons in the Deep Dorsal Horn Contribute to Mechanical Allodynia

We previously reported tVGLUT3 neurons as being potentially important for mechanical allodynia (Peirs et al., 2015). We now identify these cells as a subset of CCK-lineage neurons in laminae III–IV that are largely *Maf*$^+$ with a few *Cpne4*$^+$ neurons. Targeted CCK neurons mainly express *Cpne4* alone, or also *Maf*, and are important for punctate and dynamic allodynia in both types of injuries. The targeted tVGLUT3 population has a role primarily in dynamic mechanical allodynia, which points to the tVGLUT3$^+$/*Maf*$^+$/*Cck*$^+$ subset as being responsible. Interestingly, conditional ablation of the tVGLUT3-lineage neurons, which likely included a subset of PKCγ neurons, also did not affect punctate allodynia (Cheng et al., 2017). Both the PKCγ neurons and the targeted CCK population (lacking tVGLUT3 and PKCγ) show a partial contribution to the transmission of punctate allodynia. Full expression of the allodynia may thus require both populations (Figure 8).

Interestingly, we found that monosynaptic A-fiber inputs onto CR and PKCγ neurons come almost exclusively from Aδ but not Aβ, which is consistent with previous observations (Abraira et al., 2017), whereas the opposite observation was reported for tVGLUT3 (CCK) neurons (Peirs et al., 2015). Because all three populations are important for the full expression of mechanical

allodynia, it is likely that input from both Aβ and Aδ are required to engage the dorsal horn allodynia circuit, consistent with a recent report showing that the selective activation of Aβ-fibers only is not sufficient to induce mechanical allodynia in a model of neuropathic pain (Chamessian et al., 2019).

Corticospinal tract (CST) neurons were recently shown to play a critical role in mechanical allodynia induced by nerve injury (Liu et al., 2018). These PNs, which target neurons within the LTMR recipient zone, including CCK neurons, contribute to SNI-induced allodynia by amplifying the activity of dorsal horn neurons through a feedback loop (Liu et al., 2018). Interestingly, the neurons also express CCK and PKCγ. Since signaling by CCK itself also contributes to the transmission of mechanical allodynia at the spinal level (Wiesenfeld-Hallin et al., 2002) and CCK shows low to no expression in primary afferents normally and after injury (Figure S2G), the dorsal horn interneurons or descending supraspinal neurons, such as the CST neurons likely serve as the source of the peptide. Our findings with the kinase inhibitor closely mirror the data obtained by inhibiting the PKCγ$^+$ dorsal horn neurons, and PKCγ is also not expressed by primary afferents normally or after injury (Figure S2G). It would, nevertheless, be interesting to know what contribution the enzyme in corticospinal projections makes, if any, to the spinal circuitry.

With respect to the role of the targeted tVGLUT3 and CCK neurons in acute somatosensory behaviors, the inhibition of these populations caused a decrease in the latency to respond to sticky tape with no change in other behaviors, including the response to a cotton swab. These data suggest that the targeted neurons, which reside largely in the LTMR recipient zone, shape the timing of the behavioral response to a touch rather than alter detection sensitivity. A change in the von Frey threshold was reported with conditional ablation of the tVGLUT3-lineage neurons (Cheng et al., 2017) as well as ablation of the larger CCK population (Liu et al., 2018). Both populations include excitatory neurons in lamina II that were not targeted here and that may underlie this phenotype.

While persistent heat hypersensitivity was not a focus of the study, we show that the targeted CCK neurons have a significant role in conveying heat hypersensitivity after inflammatory injury. Since the targeted tVGLUT3 population is largely dispensable for this phenotype, the CCK neurons responsible likely belong to the *Cpne4*$^+$ subset or a not yet defined subset. TRPV1 expressing primary afferents are required for heat hypersensitivity in inflammatory models and terminate largely in laminae I, II, and deeper laminae (Caterina et al., 2000; Cavanaugh et al., 2009). The location of the targeted CCK neurons in laminae III–IV suggests that injury may increase the synaptic connectivity between TRPV1$^+$ afferents and these deeper dorsal horn neurons.

CONCLUSIONS

A key point of our study is that while the manifestations of inflammatory and neuropathic injuries with respect to mechanical allodynia behavior (pain in response to light touch) are similar, our data show that the circuitry in the dorsal horn differs. A number of studies have contributed to a model in which neuropathic injury induces spinal disinhibition, allowing innocuous mechanoreceptors to activate a polysynaptic circuit, thus turning touch into pain (Miraucourt et al., 2007; Torsney and MacDermott, 2006). This circuit includes PKCγ neurons that are normally not activated by innocuous or noxious stimuli (Lu et al., 2013; Miraucourt et al., 2007; Peirs et al., 2015), due to control by inhibitory neurons (Petitjean et al., 2015); it also includes transient central cells and vertical cells that reside in the superficial laminae dorsal to the PKCγ neurons (Figure 8). Our study confirms the critical role of PKCγ neurons in neuropathic allodynia, but it also points to other major populations located more ventrally, thus suggesting that inputs from disinhibited lamina II$_i$ neurons act in concert with these deeper neurons to transmit allodynia. Whether this same type of gating mechanism also occurs in response to inflammatory injuries, which involve neurons distinct from the PKCγ neurons, remains to be determined. Our data show that the deep dorsal horn neurons also provide a critical input to the inflammatory mechanical allodynia circuit; however, this aspect of the network may not rely on vertical cells, as CR neurons send axons directly to lamina I PNs as well (Petitjean et al., 2019; Smith et al., 2019) (Figure 8). Future investigations into the mechanical allodynia circuitry from the perspective of a network differentially activated depending on the nature of the injury will be important for fully understanding the mechanisms that give rise to this form of pain.

STAR★METHODS

Detailed methods are provided in the online version of this paper and include the following:

- KEY RESOURCES TABLE
- RESOURCE AVAILABILITY
  - Lead Contact
  - Materials Availability
  - Data and Code Availability
- EXPERIMENTAL MODEL AND SUBJECT DETAILS
  - Animals
- METHOD DETAILS
  - Experimental Design
  - Intraspinal Virus Injections
  - Tamoxifen Injections
  - Chemogenetic Activation of hM3Dq Receptor
  - Chemogenetic Activation of PSAM-GlyR Receptor
  - Tat-γV5-3 Administration
  - Behavioral Tests
  - Injury Models
  - Plantar Incision Model
  - Spared Nerve Injury (Tibial Spare)
  - Spared Nerve Injury (Sural Spare)
  - Immunohistochemistry
  - *In Situ* Hybridization
  - RNA isolation, cDNA synthesis and qPCR
  - Imaging
  - Electrophysiological recordings
  - Neuronal morphology
- QUANTIFICATION AND STATISTICAL ANALYSIS

SUPPLEMENTAL INFORMATION

Supplemental Information can be found online at https://doi.org/10.1016/j.neuron.2020.10.027.

ACKNOWLEDGMENTS

The authors thank Dr. D. Mochly-Rosen for providing the PKCγ inhibitor and tat control and Drs. D. Ginty and V. Abraira for the PKCγ^{mGFP} and PKCγ^{CreERT2} mice. We also thank Karine Herault and Samyuktha Lokanandi for help with tissue processing and immunohistochemistry (IHC) and Dr. Joe Brague for helpful comments on the manuscript. Funding was provided by the Rita Allen Foundation (United States), the American Pain Association, the American Diabetes Association, NS104964 (R.P.S.), NS096705 and AR063772 (S.E.R.), NS111643 (M.G.), NS073548 (D.W.F.), NS111791 (C.M.A.), the David Scaife Family Charitable Foundation Fellowships (United States) (P.H. and K.M.S.), and the China Scholarship Council Foundation (X.Z.).

AUTHOR CONTRIBUTIONS

C.P., S.-P.G.W., X.Z., and R.P.S. conceived the study. C.P., S.-P.G.W., D.W.F., S.J.L., and X.Z. performed the behavioral testing. C.P., S.-P.G.W., and D.W.F. generated the pain models. C.P., X.Z., M.N., P.H., C.M.A., and D.C. performed the intraspinal injections. C.P. and D.W.F. performed the i.t. injections. C.P., S.-P.G.W., X.Z., C.M.A., K.A.C., and J.Y.G. performed the IHC. C.P. and K.M.S. performed the electrophysiological recordings. C.P., P.H., and J.Y.G. performed the morphological analyses. C.M.A. performed the *in situ* hybridization. D.W.F. performed the RT-PCR. M.N. designed the viral constructs. C.P., S.-P.G.W., X.Z., K.M.S., P.H., D.W.F., C.M.A., and R.P.S. analyzed the data. G.G. and M.G. provided intellectual input. R.P.S. and C.P. wrote the manuscript with contributions from all of the other authors.

DECLARATION OF INTERESTS

The authors declare no competing interests.

Received: May 9, 2019
Revised: September 16, 2020
Accepted: October 20, 2020
Published: November 11, 2020

REFERENCES

Abraira, V.E., Kuehn, E.D., Chirila, A.M., Springel, M.W., Toliver, A.A., Zimmerman, A.L., Orefice, L.L., Boyle, K.A., Bai, L., Song, B.J., et al. (2017). The Cellular and Synaptic Architecture of the Mechanosensory Dorsal Horn. Cell *168*, 295–310.e19.

Alba-Delgado, C., El Khoueiry, C., Peirs, C., Dallel, R., Artola, A., and Antri, M. (2015). Subpopulations of PKCγ interneurons within the medullary dorsal horn revealed by electrophysiologic and morphologic approach. Pain *156*, 1714–1728.

Alba-Delgado, C., Mountadem, S., Mermet-Joret, N., Monconduit, L., Dallel, R., Artola, A., and Antri, M. (2018). 5-HT$_{2A}$ Receptor-Induced Morphological Reorganization of PKCγ-Expressing Interneurons Gates Inflammatory Mechanical Allodynia in Rat. J. Neurosci. *38*, 10489–10504.

Alexander, G.M., Rogan, S.C., Abbas, A.I., Armbruster, B.N., Pei, Y., Allen, J.A., Nonneman, R.J., Hartmann, J., Moy, S.S., Nicolelis, M.A., et al. (2009). Remote control of neuronal activity in transgenic mice expressing evolved G protein-coupled receptors. Neuron *63*, 27–39.

Artola, A., Voisin, D., and Dallel, R. (2020). PKCγ interneurons, a gateway to pathological pain in the dorsal horn. J. Neural Transm. (Vienna) *127*, 527–540.

Bautista, D.M., Jordt, S.E., Nikai, T., Tsuruda, P.R., Read, A.J., Poblete, J., Yamoah, E.N., Basbaum, A.I., and Julius, D. (2006). TRPA1 mediates the inflammatory actions of environmental irritants and proalgesic agents. Cell *124*, 1269–1282.

Bell, A.M., Gutierrez-Mecinas, M., Stevenson, A., Casas-Benito, A., Wildner, H., West, S.J., Watanabe, M., and Todd, A.J. (2020). Expression of green fluorescent protein defines a specific population of lamina II excitatory interneurons in the GRP:eGFP mouse. Sci. Rep. *10*, 13176.

Bouhassira, D., Attal, N., Alchaar, H., Boureau, F., Brochet, B., Bruxelle, J., Cunin, G., Fermanian, J., Ginies, P., Grun-Overdyking, A., et al. (2005). Comparison of pain syndromes associated with nervous or somatic lesions and development of a new neuropathic pain diagnostic questionnaire (DN4). Pain *114*, 29–36.

Brennan, T.J., Zahn, P.K., and Pogatzki-Zahn, E.M. (2005). Mechanisms of incisional pain. Anesthesiol. Clin. North America *23*, 1–20.

Caterina, M.J., Leffler, A., Malmberg, A.B., Martin, W.J., Trafton, J., Petersen-Zeitz, K.R., Koltzenburg, M., Basbaum, A.I., and Julius, D. (2000). Impaired nociception and pain sensation in mice lacking the capsaicin receptor. Science *288*, 306–313.

Cavanaugh, D.J., Lee, H., Lo, L., Shields, S.D., Zylka, M.J., Basbaum, A.I., and Anderson, D.J. (2009). Distinct subsets of unmyelinated primary sensory fibers mediate behavioral responses to noxious thermal and mechanical stimuli. Proc. Natl. Acad. Sci. USA *106*, 9075–9080.

Chamessian, A., Young, M., Qadri, Y., Berta, T., Ji, R.R., and Van de Ven, T. (2018). Transcriptional Profiling of Somatostatin Interneurons in the Spinal Dorsal Horn. Sci. Rep. *8*, 6809.

Chamessian, A., Matsuda, M., Young, M., Wang, M., Zhang, Z.J., Liu, D., Tobin, B., Xu, Z.Z., Van de Ven, T., and Ji, R.R. (2019). Is Optogenetic Activation of Vglut1-Positive Aβ Low-Threshold Mechanoreceptors Sufficient to Induce Tactile Allodynia in Mice after Nerve Injury? J. Neurosci. *39*, 6202–6215.

Chaplan, S.R., Bach, F.W., Pogrel, J.W., Chung, J.M., and Yaksh, T.L. (1994). Quantitative assessment of tactile allodynia in the rat paw. J. Neurosci. Methods *53*, 55–63.

Cheng, L., Duan, B., Huang, T., Zhang, Y., Chen, Y., Britz, O., Garcia-Campmany, L., Ren, X., Vong, L., Lowell, B.B., et al. (2017). Identification of spinal circuits involved in touch-evoked dynamic mechanical pain. Nat. Neurosci. *20*, 804–814.

Cordero-Erausquin, M., Inquimbert, P., Schlichter, R., and Hugel, S. (2016). Neuronal networks and nociceptive processing in the dorsal horn of the spinal cord. Neuroscience *338*, 230–247.

Cowie, A.M., Moehring, F., O'Hara, C., and Stucky, C.L. (2018). Optogenetic Inhibition of CGRPα Sensory Neurons Reveals Their Distinct Roles in Neuropathic and Incisional Pain. J. Neurosci. *38*, 5807–5825.

Cui, L., Miao, X., Liang, L., Abdus-Saboor, I., Olson, W., Fleming, M.S., Ma, M., Tao, Y.X., and Luo, W. (2016). Identification of Early RET+ Deep Dorsal Spinal Cord Interneurons in Gating Pain. Neuron *91*, 1413.

Decosterd, I., and Woolf, C.J. (2000). Spared nerve injury: an animal model of persistent peripheral neuropathic pain. Pain *87*, 149–158.

Duan, B., Cheng, L., Bourane, S., Britz, O., Padilla, C., Garcia-Campmany, L., Krashes, M., Knowlton, W., Velasquez, T., Ren, X., et al. (2014). Identification of spinal circuits transmitting and gating mechanical pain. Cell *159*, 1417–1432.

Finnerup, N.B., Attal, N., Haroutounian, S., McNicol, E., Baron, R., Dworkin, R.H., Gilron, I., Haanpää, M., Hansson, P., Jensen, T.S., et al. (2015). Pharmacotherapy for neuropathic pain in adults: a systematic review and meta-analysis. Lancet Neurol. *14*, 162–173.

Gao, Y.J., and Ji, R.R. (2010). Light touch induces ERK activation in superficial dorsal horn neurons after inflammation: involvement of spinal astrocytes and JNK signaling in touch-evoked central sensitization and mechanical allodynia. J. Neurochem. *115*, 505–514.

Gatto, G., Bourane, S., Ren, X., Di Costanzo, S., Fenton, P., Halder, P., Seal, R.P., and Goulding, M. (2020). A functional topographic map for spinal sensorimotor reflexes. Neuron *109*.

Gatto, G., Smith, K.M., Ross, S.E., and Goulding, M. (2019). Neuronal diversity in the somatosensory system: bridging the gap between cell type and function. Curr. Opin. Neurobiol. *56*, 167–174.

Grimes, W.N., Seal, R.P., Oesch, N., Edwards, R.H., and Diamond, J.S. (2011). Genetic targeting and physiological features of VGLUT3+ amacrine cells. Vis. Neurosci. *28*, 381–392.

Groc, L., Heine, M., Cognet, L., Brickley, K., Stephenson, F.A., Lounis, B., and Choquet, D. (2004). Differential activity-dependent regulation of the lateral mobilities of AMPA and NMDA receptors. Nat. Neurosci. *7*, 695–696.

Gutierrez-Mecinas, M., Bell, A.M., Shepherd, F., Polgár, E., Watanabe, M., Furuta, T., and Todd, A.J. (2019a). Expression of cholecystokinin by neurons in mouse spinal dorsal horn. J. Comp. Neurol. *527*, 1857–1871.

Gutierrez-Mecinas, M., Davis, O., Polgár, E., Shahzad, M., Navarro-Batista, K., Furuta, T., Watanabe, M., Hughes, D.I., and Todd, A.J. (2019b). Expression of Calretinin Among Different Neurochemical Classes of Interneuron in the Superficial Dorsal Horn of the Mouse Spinal Cord. Neuroscience *398*, 171–181.

Häring, M., Zeisel, A., Hochgerner, H., Rinwa, P., Jakobsson, J.E.T., Lönnerberg, P., La Manno, G., Sharma, N., Borgius, L., Kiehn, O., et al. (2018). Neuronal atlas of the dorsal horn defines its architecture and links sensory input to transcriptional cell types. Nat. Neurosci. *21*, 869–880.

Huang, T., Lin, S.H., Malewicz, N.M., Zhang, Y., Zhang, Y., Goulding, M., LaMotte, R.H., and Ma, Q. (2019). Identifying the pathways required for coping behaviours associated with sustained pain. Nature *565*, 86–90.

Hughes, D.I., and Todd, A.J. (2020). Central nervous system targets: inhibitory interneurons in the spinal cord. Neurotherapeutics.

Lennertz, R.C., Kossyreva, E.A., Smith, A.K., and Stucky, C.L. (2012). TRPA1 mediates mechanical sensitization in nociceptors during inflammation. PLOS ONE *7*, e43597.

Liu, Y., Latremoliere, A., Li, X., Zhang, Z., Chen, M., Wang, X., Fang, C., Zhu, J., Alexandre, C., Gao, Z., et al. (2018). Touch and tactile neuropathic pain sensitivity are set by corticospinal projections. Nature *561*, 547–550.

Livak, K.J., and Schmittgen, T.D. (2001). Analysis of relative gene expression data using real-time quantitative PCR and the 2(-Delta Delta C(T)) Method. Methods *25*, 402–408.

Lu, Y., Dong, H., Gao, Y., Gong, Y., Ren, Y., Gu, N., Zhou, S., Xia, N., Sun, Y.Y., Ji, R.R., and Xiong, L. (2013). A feed-forward spinal cord glycinergic neural circuit gates mechanical allodynia. J. Clin. Invest. *123*, 4050–4062.

Magnus, C.J., Lee, P.H., Atasoy, D., Su, H.H., Looger, L.L., and Sternson, S.M. (2011). Chemical and genetic engineering of selective ion channel-ligand interactions. Science *333*, 1292–1296.

Malmberg, A.B., Chen, C., Tonegawa, S., and Basbaum, A.I. (1997). Preserved acute pain and reduced neuropathic pain in mice lacking PKCgamma. Science *278*, 279–283.

Matsuda, M., Huh, Y., and Ji, R.R. (2019). Roles of inflammation, neurogenic inflammation, and neuroinflammation in pain. J. Anesth. *33*, 131–139.

Miraucourt, L.S., Dallel, R., and Voisin, D.L. (2007). Glycine inhibitory dysfunction turns touch into pain through PKCgamma interneurons. PLOS ONE *2*, e1116.

Miyamichi, K., Shlomai-Fuchs, Y., Shu, M., Weissbourd, B.C., Luo, L., and Mizrahi, A. (2013). Dissecting local circuits: parvalbumin interneurons underlie broad feedback control of olfactory bulb output. Neuron *80*, 1232–1245.

Moehring, F., Halder, P., Seal, R.P., and Stucky, C.L. (2018). Uncovering the Cells and Circuits of Touch in Normal and Pathological Settings. Neuron *100*, 349–360.

Pagani, M., Albisetti, G.W., Sivakumar, N., Wildner, H., Santello, M., Johannssen, H.C., and Zeilhofer, H.U. (2019). How Gastrin-Releasing Peptide Opens the Spinal Gate for Itch. Neuron *103*, 102–117.e5.

Peirs, C., and Seal, R.P. (2016). Neural circuits for pain: recent advances and current views. Science *354*, 578–584.

Peirs, C., Patil, S., Bouali-Benazzouz, R., Artola, A., Landry, M., and Dallel, R. (2014). Protein kinase C gamma interneurons in the rat medullary dorsal horn: distribution and synaptic inputs to these neurons, and subcellular localization of the enzyme. J. Comp. Neurol. *522*, 393–413.

Peirs, C., Williams, S.P., Zhao, X., Walsh, C.E., Gedeon, J.Y., Cagle, N.E., Goldring, A.C., Hioki, H., Liu, Z., Marell, P.S., and Seal, R.P. (2015). Dorsal Horn Circuits for Persistent Mechanical Pain. Neuron *87*, 797–812.

Peirs, C., Dallel, R., and Todd, A.J. (2020). Recent advances in our understanding of the organization of dorsal horn neuron populations and their contribution to cutaneous mechanical allodynia. J. Neural Transm. (Vienna) *127*, 505–525.

Petitjean, H., Bourojeni, F.B., Tsao, D., Davidova, A., Sotocinal, S.G., Mogil, J.S., Kania, A., and Sharif-Naeini, R. (2019). Recruitment of Spinoparabrachial Neurons by Dorsal Horn Calretinin Neurons. Cell Rep. *28*, 1429–1438.e4.

Petitjean, H., Pawlowski, S.A., Fraine, S.L., Sharif, B., Hamad, D., Fatima, T., Berg, J., Brown, C.M., Jan, L.Y., Ribeiro-da-Silva, A., et al. (2015). Dorsal Horn Parvalbumin Neurons Are Gate-Keepers of Touch-Evoked Pain after Nerve Injury. Cell Rep. *13*, 1246–1257.

Seal, R.P., Wang, X., Guan, Y., Raja, S.N., Woodbury, C.J., Basbaum, A.I., and Edwards, R.H. (2009). Injury-induced mechanical hypersensitivity requires C-low threshold mechanoreceptors. Nature *462*, 651–655.

Shields, S.D., Eckert, W.A., 3rd, and Basbaum, A.I. (2003). Spared nerve injury model of neuropathic pain in the mouse: a behavioral and anatomic analysis. J. Pain *4*, 465–470.

Singhmar, P., Huo, X., Eijkelkamp, N., Berciano, S.R., Baameur, F., Mei, F.C., Zhu, Y., Cheng, X., Hawke, D., Mayor, F., Jr., et al. (2016). Critical role for Epac1 in inflammatory pain controlled by GRK2-mediated phosphorylation of Epac1. Proc. Natl. Acad. Sci. USA *113*, 3036–3041.

Sluka, K.A. (2002). Stimulation of deep somatic tissue with capsaicin produces long-lasting mechanical allodynia and heat hypoalgesia that depends on early activation of the cAMP pathway. J. Neurosci. *22*, 5687–5693.

Smith, K.M., Boyle, K.A., Madden, J.F., Dickinson, S.A., Jobling, P., Callister, R.J., Hughes, D.I., and Graham, B.A. (2015). Functional heterogeneity of calretinin-expressing neurons in the mouse superficial dorsal horn: implications for spinal pain processing. J. Physiol. *593*, 4319–4339.

Smith, K.M., Browne, T.J., Davis, O.C., Coyle, A., Boyle, K.A., Watanabe, M., Dickinson, S.A., Iredale, J.A., Gradwell, M.A., Jobling, P., et al. (2019). Calretinin positive neurons form an excitatory amplifier network in the spinal cord dorsal horn. eLife *8*, e49190.

Sun, S., Xu, Q., Guo, C., Guan, Y., Liu, Q., and Dong, X. (2017). Leaky Gate Model: Intensity-Dependent Coding of Pain and Itch in the Spinal Cord. Neuron *93*, 840–853.e5.

Sweitzer, S.M., Wong, S.M., Peters, M.C., Mochly-Rosen, D., Yeomans, D.C., and Kendig, J.J. (2004). Protein kinase C epsilon and gamma: involvement in formalin-induced nociception in neonatal rats. J. Pharmacol. Exp. Ther. *309*, 616–625.

Todd, A.J. (2017). Identifying functional populations among the interneurons in laminae I-III of the spinal dorsal horn. Mol. Pain *13*, 1–19.

Torsney, C., and MacDermott, A.B. (2006). Disinhibition opens the gate to pathological pain signaling in superficial neurokinin 1 receptor-expressing neurons in rat spinal cord. J. Neurosci. *26*, 1833–1843.

Usoskin, D., Furlan, A., Islam, S., Abdo, H., Lönnerberg, P., Lou, D., Hjerling-Leffler, J., Haeggström, J., Kharchenko, O., Kharchenko, P.V., et al. (2015). Unbiased classification of sensory neuron types by large-scale single-cell RNA sequencing. Nat. Neurosci. *18*, 145–153.

Wiesenfeld-Hallin, Z., Xu, X.J., and Hökfelt, T. (2002). The role of spinal cholecystokinin in chronic pain states. Pharmacol. Toxicol. *91*, 398–403.

Xu, Y., Lopes, C., Qian, Y., Liu, Y., Cheng, L., Goulding, M., Turner, E.E., Lima, D., and Ma, Q. (2008). Tlx1 and Tlx3 coordinate specification of dorsal horn pain-modulatory peptidergic neurons. J. Neurosci. *28*, 4037–4046.

Yasaka, T., Tiong, S.Y., Polgár, E., Watanabe, M., Kumamoto, E., Riddell, J.S., and Todd, A.J. (2014). A putative relay circuit providing low-threshold mechanoreceptive input to lamina I projection neurons via vertical cells in lamina II of the rat dorsal horn. Mol. Pain *10*, 3.

STAR★METHODS

KEY RESOURCES TABLE

REAGENT or RESOURCE	SOURCE	IDENTIFIER
Antibodies		
Guinea Pig polyclonal anti-PKCγ (1:500, IHC)	Frontier Institute	AF350
Mouse monoclonal anti-Calretinin (1:1000, IHC)	Swant	RRID: AB_10000320
Mouse monoclonal anti-NeuN (1:1000, IHC)	Chemicon	RRID: AB_2298772
anti-hPax2 Affinity Purified Goat IgG (1:200, IHC)	R&D Systems	RRID: AB_10889828
Chicken anti-GFP (1:1000, IHC)	Life Technologies	RRID: AB_2534023
Rabbit anti-GFP (1:1000, IHC)	Molecular Probes	RRID: AB_221570
α-Bungarotoxin Alexa Fluor 647 conjugate (1:3000, IHC)	Life Technologies	Cat: B35450 LOT: 1712139
α-Bungarotoxin Alexa Fluor 488 conjugate (1:3000, IHC)	Life Technologies	Cat: B13422 LOT: 1843685
AffiniPure Donkey anti-Mouse DyLight 405 (1:500, IHC)	Jackson ImmunoResearch	RRID: AB_2340839
AffiniPure Donkey anti-Mouse Alexa Fluor 488 (1:500, IHC)	Jackson ImmunoResearch	RRID: AB_2340846
AffiniPure Donkey anti-Mouse Alexa Fluor 594 (1:500, IHC)	Jackson ImmunoResearch	RRID: AB_2340854
AffiniPure Donkey anti-Mouse Alexa Fluor 647 (1:500, IHC)	Jackson ImmunoResearch	RRID: AB_2340862
AffiniPure Donkey anti-Rabbit Alexa Fluor 488 (1:500, IHC)	Jackson ImmunoResearch	RRID: AB_2313584
AffiniPure Donkey anti-Rabbit Alexa Fluor 594 (1:500, IHC)	Jackson ImmunoResearch	RRID: AB_2340623
AffiniPure Donkey anti-Rabbit Alexa Fluor 647 (1:500, IHC)	Jackson ImmunoResearch	RRID: AB_2492288
AffiniPure Donkey anti-Chicken Alexa Fluor 488 (1:500, IHC)	Jackson ImmunoResearch	RRID: AB_2340375
AffiniPure Donkey anti-Goat DyLight 405 (1:500, IHC)	Jackson ImmunoResearch	RRID: AB_2340426
AffiniPure Donkey anti-Goat Alexa Fluor 488 (1:500, IHC)	Jackson ImmunoResearch	RRID: AB_2340428
AffiniPure Donkey anti-Goat Alexa Fluor 647 (1:500, IHC)	Jackson ImmunoResearch	RRID: AB_2340436
AffiniPure Donkey anti-Guinea Pig DyLight 405 (1:500, IHC)	Jackson ImmunoResearch	RRID: AB_2340470
AffiniPure Donkey anti-Guinea Pig Alexa Fluor 488 (1:500, IHC)	Jackson ImmunoResearch	RRID: AB_2340472
AffiniPure Donkey anti-Guinea Pig Cy3 conjugate (1:500, IHC)	Jackson ImmunoResearch	RRID: AB_2340460
AffiniPure Donkey anti-Guinea Pig Alexa Fluor 594 (1:500, IHC)	Jackson ImmunoResearch	RRID: AB_2340474
AffiniPure Donkey anti-Guinea Pig Alexa Fluor 647	Jackson ImmunoResearch	RRID: AB_2340476
Bacterial and Virus Strains		
AAV8.hSyn.DIO.EGFP	UNC Vector Core and Vigene Biosciences	N/A
AAV8.hSyn.FLEX.PSAML141F-GlyR.IRES.EGFP	UNC Custom	N/A
AAV8.hSyn.DIO.hM3d(Gq)-mCherry	UNC Roth Collection	N/A
AAVDJ.pCAG.FLEX.PSAML141F-GlyR	Vigene Biosciences Custom	N/A
Chemicals, Peptides, and Recombinant Proteins		
Clozapine-N-Oxide	Enzo Life Science	BML-NS105-0025
PSEM^{89S} (S)-2,5-Dimethoxy-N-(quinuclidine-3-yl)benzamide	Apex Scientific	1221570-55-3
λ-Carrageenan	Sigma Aldrich	22049-5G-F
Capsaicin	Sigma Aldrich	M2028
Complete Freund's Adjuvant	Sigma Aldrich	F5881
Allyl Isothiocyanate (Mustard Oil)	Sigma Aldrich	377430
Ketathesia	Henry Schein Animal Health	056334
AnaSed (Xylazine)	Henry Schein Animal Health	033197
Isothesia (Isoflurane)	Henry Schein Animal Health	029405
Formalin	Sigma	181090010

(*Continued on next page*)

Continued

REAGENT or RESOURCE	SOURCE	IDENTIFIER
TSA Biotin System	Perkin Elmer	NEL700A001KT
Tamoxifen	Sigma-Aldrich	T5648
Tat-γV5-3	Dr. Mochley-Rosen. (Sweitzer et al., 2004)	N/A
Experimental Models: Organisms/Strains		
Cck$^{tm1.1(cre)Zjh/J}$ (CCK^{Cre})	Jackson Laboratories	RRID: IMSR_JAX:012706
Calb$^{2tm1(cre)Zjh/J}$ (CR^{Cre})	Jackson Laboratories	RRID: IMSR_JAX:010774
Tg(Slc17a8-icre)1Edw/SealJ (VGLUT3^{iCre})	Jackson Labs Rebecca Seal	RRID: IMSR_JAX:018147
Tg(Slc17a8-EGFP)1Edw/SealJ (VGLUT3^{eGFP})	Jackson Labs Rebecca Seal	RRID: IMSR_JAX:018148
PKCγ^{mGFP}	David Ginty (Abraira et al., 2017)	N/A
PKCγ^{CreERT2}	David Ginty (Abraira et al., 2017)	N/A
B6.Cg-*Gt(ROSA)26Sor*$^{tm14(CAG-tdTomato)Hze}$/J (tdTomato)	Jackson Laboratories	RRID: IMSR_JAX:007914
Tlx3$^{tm1(cre)Qima}$	Qiufu Ma (Xu et al., 2008)	N/A
C57BL/6J	Jackson Laboratories	RRID: IMSR_JAX:000664
Oligonucleotides		
qPCR primers, see Table S1	This paper	N/A
Cholecystokinin (Cck) RNAscope probe (C2, C3 channels)	ACDBio	402271
Copine-4 (Cpne4) RNAscope probe (C1 channel)	ACDBio	474721
v-maf musculoaponeurotic fibrosarcoma oncogene homolog (avian) (Maf) RNAscope probe (C3 channel)	ACDBio	412951
Thyrotropin Releasing Hormone (Trh) RNAscope probe (C3 channel)	ACDBio	436811
Tachykinin precursor 1 (Tac1) RNAscope probe (C1 channel)	ACDBio	410351
Tachykinin2 (Tac2) RNAscope probe (C3 channel)	ACDBio	446391
Lamp5 RNAscope probe (C3 channel)	ACDBio	451071
Gastrin releasing peptide (Grp) RNAscope probe (C1 channel)	ACDBio	317861
Recombinant DNA		
pCAG-Flex-TCB	Miyamichi et al., 2013	Addgene (#48332)
Software and Algorithms		
PRISM v7 and v8	GraphPad	RRID: SCR_002798; https://www.graphpad.com/scientific-software/prism/
NIS-Elements	Nikon	RRID: SCR_014329; https://www.microscope.healthcare.nikon.com/
Fiji (ImageJ)	NIH	RRID: SCR_002285; https://imagej.nih.gov/ij/
Axon pCLAMP v10	Molecular Devices	RRID: SCR_011323; https://www.moleculardevices.com/products/axon-patch-clamp-system
Canvas X	Canvas GTX	RRID: SCR_014312; https://www.canvasgfx.com/en/products/canvas-x/
Corel Draw X7	Corel Corporation	RRID: SCR_014235; https://www.coreldraw.com/en/

RESOURCE AVAILABILITY

Lead Contact

Further information and requests for resources and reagents should be directed to and will be fulfilled by the Lead Contact, Rebecca Seal (rpseal@pitt.edu).

Materials Availability

All unique reagents generated in this study are available from the Lead Contact with a Materials Transfer Agreement.

Data and Code Availability

This study did not generate datasets/code.

EXPERIMENTAL MODEL AND SUBJECT DETAILS

Animals

All animals were kept on a standard 12:12 light/dark cycle in micro-isolator caging racks (Allentown Caging) with food and water provided *ad libitum* and were treated in accordance with protocols approved by the University of Pittsburgh's Institutional Animal Care and Use Committee. Mouse strains obtained from Jackson Laboratories include C57BL/6J (RRID: IMSR_JAX:000664), tdTomato (Ai14) (RRID: IMSR_JAX:007914), CR^{Cre} (RRID: IMSR_JAX:010774) and CCK^{Cre} (RRID: IMSR_JAX:012706). Dr. Qiufu Ma supplied the $Tlx3^{Cre}$ line (Xu et al., 2008), Drs. David Ginty and Victoria Abraira provided the $PKC\gamma^{mGFP}$ and $PKC\gamma^{CreERT2}$ mice (Abraira et al., 2017). $VGLUT3^{Cre}$ (RRID: IMSR_JAX:018147) and $VGLUT3^{EGFP}$ (RRID: IMSR_JAX:018148 were generated as previously described (Grimes et al., 2011; Peirs et al., 2015; Seal et al., 2009). Mice ranging in age from 1 week to 6 months were used for this study. Both male and female mice were used in this study. No significant sex differences were observed.

METHOD DETAILS

Experimental Design

For behavioral experiments, measurements were taken blinded to condition (e.g., PKCγ inhibitor versus control peptide, saline versus $PSEM^{89S}$, except when only $PSEM^{89S}$ was injected). Sample size was based on Peirs et al., 2015. Mice from multiple litters born within 2 weeks of each other were used in the same behavioral experiments.

Intraspinal Virus Injections

Mice were injected as previously described (Peirs et al., 2015). Briefly, P7-10 (for $VGLUT3^{Cre}$) or P21-22 (for CR^{Cre}, $PKC\gamma^{CreERT2}$, and CCK^{Cre}) mice were anesthetized with 2.5% isoflurane. A midline incision along the left lumbar vertebrae was carefully performed until the spinal cord was visible from the intervertebral spaces between T12 and T13 vertebral spines. No laminectomy was performed to minimize trauma. A glass microelectrode with ~50 μm tip was inserted between L3-L4 spinal cord to a depth of −250 μm below the dura using a stereotaxic frame, taking care to avoid the posterior spinal arteries. One μl of viral solution was slowly infused over a period of 5 minutes using a stereotaxic injector. The micropipette was left in place for 3 minutes after infusion then slowly removed. The *lassimus dorsi* were then sutured over the incision to protect the spinal cord, and the skin closed with silk sutures. Behavior tests were performed 3-4 weeks after viral inoculation to allow maximal and stable expression. Electrophysiological recordings were performed 1-2 weeks after viral infection. AAV8.hSyn.DiO.EGFP (4.9 × 10e12 vg/ml) was purchased from UNC vector core (Chapel Hill, NC) or was (3e13 vg/ml) custom made at Vigene Biosciences. AAV8.hSyn.DiO.hM3Dq-mCherry (5.7e12 vg/ml) was purchased from UNC vector core. The AAV8.hSyn.FLEX-rev-$PSAM^{L141F}$-GlyR.IRES.GFP (7e12 vg/ml) was custom made by UNC Vector core based on plasmid material developed by Scott Sternson and provided by Addgene. pCAG-FLEX-rev-$PSAM^{L141F}$-GlyR (1.01e13 vg/ml) was generated by subcloning rev-$PSAM^{L141F}$-GlyR sequence into pCAG-Flex vector purchased from Addgene (#48332)(Miyamichi et al., 2013). This 1.8 kb CAG promoter includes the chicken β-actin promoter, CMV enhancer and an intron. Due to limited AAV packaging capacity, IRES-GFP sequence from the rev-$PSAM^{L141F}$-GlyR- IRES-GFP was not included. Plasmid was packaged into AAVDJ by Vigene Biosciences.

Tamoxifen Injections

Tamoxifen (T5648; Sigma-Aldrich) was prepared by dissolving in 100% ethanol, vortexing with corn oil (20 mg/ml) and then evaporating off ethanol using a SpeedVac concentrator. Mice were injected via intraperitoneal (*i.p.*) with 50-75 μL once per day for 5 days beginning 2-7 days after intraspinal injection.

Chemogenetic Activation of hM3Dq Receptor

Behavior thresholds were performed as described above in AAV8.hSyn.DIO.hM3Dq-mCherry injected mice both before and after administration of the ligand, clozapine-N-Oxide (CNO, Enzo BML-NS105-0025). CNO (5 mg/kg) was injected intraperitoneally 30 minutes prior to testing.

Chemogenetic Activation of PSAM-GlyR Receptor

Somatosensory and motor behaviors were measured in PSAM-GlyR expressing mice injected intraperitoneally with saline or the ligand $PSEM^{89S}$ (30-50 mg/kg) dissolved in saline 15 minutes prior to testing both before (for baseline assays) and after (for persistent pain assays) injury.

Tat-γV5-3 Administration

Mice were lightly anesthetized with 1.5% inhaled isoflurane and given a 5 μL intrathecal injection of tat-γV5-3 or unconjugated tat-control peptide dissolved in sterile aCSF solution. Behaviors were assessed 15 minutes after injection of the peptide.

Behavioral Tests

Paw Withdrawal Threshold to von Frey Filaments

Mice were tested as previously described (Peirs et al., 2015). Briefly, mice were habituated to opaque Plexiglas chambers on a wire mesh table for 30 minutes the day before and immediately prior to testing. Testing was performed using a set of calibrated Semmes-Weinstein monofilaments using the Up-Down method, beginning with a 0.4 g filament (Chaplan et al., 1994). The 50% paw withdraw threshold (PWT) was determined for each mouse on one or both hind paws. Each filament was gently applied to the plantar surface of the hind paw for 3 s or until a response such as a sharp withdrawal, shaking or licking of the limb was observed. Incidents of rearing or normal ambulation during filament application were not counted. Filaments were applied at five-minute intervals until thresholds were determined.

Paw Withdrawal Threshold to Pressure

Mice were lightly restrained by hand such that their rear legs were allowed to freely hang. Using a Pressure Application Measurement device (Ugo Basile) the hind paw was grasped between the experimenter's forefinger and thumb (with pressure transducer on the thumb), and force was slowly applied to the paw until the mouse struggled or flicked its limb (paw withdrawal threshold, PWT). The final force in grams was recorded. Each mouse was tested on the left and right paw for three trials with a ten-minute inter-trial interval between applications, and the three results averaged for each paw.

Dynamic Mechanical Allodynia (Cotton Swab Method)

The test was performed as described previously (Peirs et al., 2015). Briefly, animals were first placed in a square Plexiglas chamber on top of a wire mesh table and allowed to acclimate to this testing arena for 1 hour the day before and 30 minutes prior to testing. Using forceps, the head of a cotton swab was teased and puffed out until it reached approximately three times its original size. The cotton swab was lightly run across the surface of the hind paw from heel to toe. If the animal reacted (lifting, shaking, licking of the paw) a positive response was recorded. A negative response was recorded if the animal showed no such behavior. The application was repeated 6 times with a 3-minute interval between applications, and a percentage frequency of response determined for each animal.

Plantar Heat Test (Hargreaves Method)

Mice were tested as previously described (Peirs et al., 2015). Animals were placed in an acrylic chamber on a temperature-regulated glass top table (set to 30°C) and allowed to acclimate to the test chamber for 1 hour the day before and 30 minutes the day of testing. Using a Plantar Analgesia Meter (IITC, 20% intensity) a radiant heat source of constant intensity was focused on the plantar surface of the hind paw and the latency to paw withdrawal measured (PWL). The heat source was shut off upon paw withdrawal or after 20 s of exposure to prevent injury. The test was repeated 3 times on each hind paw with a 5-minute interval between tests and the results for each paw averaged together.

Pinprick test

Mice were tested as previously described (Peirs et al., 2015). Briefly, animals were first placed in a square Plexiglas chamber on top of a wire mesh table. Animals were acclimated to this testing arena for 1 hour on the day prior to testing and for an additional 30 minutes immediately before testing. A small insect pin (tip diameter = 0.03 mm) was applied with minimal pressure to the plantar surface of the left hind paw, taking care not to penetrate the skin. If the animal showed aversive behavior (lifting, shaking, licking of the paw) a positive response was recorded. A negative response was recorded if the animal showed no such reaction within 2 s of application. The application was repeated 10 times with a 5-minute interval between applications, and a percentage positive response determined for each animal.

Sticky Tape Test

Animals were placed in an empty plastic chamber and allowed to acclimate for 15-20 minutes. A ¼ inch diameter adhesive paper circle was then applied to the plantar surface of the left hind paw covering the footpads, and the animals were immediately placed back in the chamber. The animals were observed until they demonstrated a behavioral response to the adhesive tape, and the latency in seconds to respond was recorded. Inspection of the paw, shaking of the paw or attempting to remove the tape were all considered valid responses. Each animal was habituated 3 times over 3 days and then tested 3 times with a 5-mintute interval between tests, and the three values averaged for each animal.

Paw Lifting/Guarding Assays

Mice were placed in a glass chamber with a smooth plastic floor and injected intraperitoneally with 5 mg/kg CNO in saline or saline only. The mouse was allowed to acclimate to the chamber for 15 minutes post-injection and then recorded by video for 10 minutes. The videos were then analyzed for incidents of the mouse visibly lifting or shaking its paw outside of ambulation (paw withdrawal), and time in which the paw was held such that the glabrous surface was not in contact with the floor or held in an abnormal posture tucked under the body (guarding).

Rotarod Test

Mice were habituated to the test room for 15 minutes and then placed against the direction of rotation and the rod set to rotate at an increasing speed from 4 RPM to 40 RPM over 120 s. When a mouse fell from the rod, the time and revolutions per minute (RPM) at fall were recorded. The test was repeated 3 times with a 5-minute interval between tests and the results averaged together.

Injury Models

Carrageenan-induced inflammation

Mice were lightly anesthetized via inhaled 2.5% isoflurane and injected with 20 μL of 3% λ-Carrageenan (Sigma 22049) dissolved in sterile 0.9% NaCl into the plantar surface of the left hind paw. Somatosensory assays were performed the day before and 24 hours after injection.

Intradermal Capsaicin Injection

Mice were lightly anesthetized via inhaled 2.5% Isoflurane and injected with 5 μL of 0.5% Capsaicin (Sigma) in the glabrous surface of the hind paw proximal to the ankle joint. Paw withdrawal thresholds were measured on the paw pads away from the primary injection site. Paw withdrawal thresholds were assessed two hours after injection.

Allyl Isothiocyanate (Mustard Oil) Injection

Mice were lightly anesthetized via inhaled 2.5% Isoflurane and injected with 5 μL of 10% AITC (Sigma) in the plantar surface of the hind paw. Paw withdrawal thresholds were assessed 45 minutes after injection.

Complete Freund's Adjuvant (CFA) Injection

Mice were lightly anesthetized via inhaled 2.5% Isoflurane and injected with 10 μL of an emulsion of equal parts Complete Freund's Adjuvant (Sigma F5881) and sterile 0.9% NaCl in the glabrous surface of the hind paw. Somatosensory behaviors were assessed five days after injection.

Plantar Incision Model

Procedure was performed as previously described (Seal et al., 2009). Animals were anesthetized with 2.5% inhaled Isoflurane. The hind paw was positioned such that the entire glabrous surface of the paw was accessible and cleaned thoroughly with Betadine iodine solution followed by 70% ethanol. A small (~2mm) incision was made in the glabrous surface of the paw between the ankle and walking pads, through the underlying skin, facia and muscle. The skin and muscle were then each closed by 2 horizontal mattress sutures using 6-0 silk suture (Henry Schein). Once closed, the incision was treated with triple antibiotic ointment. Somatosensory behaviors were assessed 3 days after incision. Any animal with an incision that had not healed shut or showing any signs of infection or significant inflammation was excluded from the study.

Spared Nerve Injury (Tibial Spare)

Surgery was performed as described (Shields et al., 2003). Briefly, mice were deeply anesthetized using a mix of 100 mg/kg ketamine and 20 mg/kg xylazine by intraperitoneal injection or with 2.5% inhaled Isoflurane. The left hind limb was shaved with trimmers and sterilized with betadine and ethanol. A small incision was made in the skin of the leg proximal to the knee and the skin and underlying muscle opened by blunt dissection to expose the three branches of the sciatic nerve. The peroneal and sural branches were tightly ligated with 6-0 nylon sutures and transected below the ligature, and a 2-3 mm section distal to the ligature was removed. Care was taken to avoid disturbing the tibial nerve, which was left intact. The muscle tissue was closed back over the nerves and the skin sutured shut with 6-0 nylon sutures. Paw withdrawal thresholds to von Frey filaments were determined the day before and 1 week after surgery.

Spared Nerve Injury (Sural Spare)

Sural Spared Nerve Injury was performed in identical fashion to the tibial spare model (above), except that the tibial and peroneal branches of the sciatic nerve were instead ligated with a single suture and transected, leaving the Sural nerve intact (Decosterd and Woolf, 2000). Paw withdrawal thresholds to von Frey filaments and response to a cotton swab were determined the day before and 1, 2, and 6 weeks after surgery.

Immunohistochemistry

Mice were deeply anesthetized with a mix of ketamine and xylazine and then transcardially perfused with phosphate-buffered saline (PBS) followed by 4% paraformaldehyde (PFA). A laminectomy was performed, and the spinal cord and dorsal root ganglia harvested. Tissues were post-fixed in 4% PFA overnight, cryo-protected in 30% sucrose and then cut with a cryostat (Microm HM550) into 10-30 μm sections placed directly onto poly-lysine coated slides or into wells containing PBS. For fluorescent immunostaining, spinal cord slices were blocked with 5% normal donkey serum (NDS) in PBS + 1% triton-X (PBS-T) for 1 hour at room temperature (RT) then incubated in primary antibody diluted in 5% NDS in PBS-T overnight at 4°C. Sections were then washed in PBS and incubated in AlexaFluor secondary antibodies (Jackson ImmunoResearch, see Key Resources Table) diluted 1:1000 in 1% NDS in PBS-T, for 1-2 hours at RT. Slices were then washed in PBS and coverslipped with Fluoromount-G or Fluoromount-G containing DAPI (Southern Biotech 0100-200).

The following primary antibodies were used for immunofluorescence staining at the following dilutions: anti-PKCγ raised in guinea pig (1:500; Frontier Institute AF350), anti-calretinin raised in mouse (1:1000; RRID: AB_10000320), anti-Pax2 raised in Goat (1:200; RRID: AB_10889828), anti-EGFP raised in rabbit (1:1000, RRID: AB_221570), anti-GFP raised in chicken, (1:1000, RRID: AB_2534023) anti-NeuN raised in mouse (1:1000, RRID: AB_2298772). We also used α–bungarotoxin conjugated to Alexa-647 (1:1000; ThermoFisher B35450), α–bungarotoxin conjugated to Alexa 488 (1:1000; ThermoFisher B13422), and Streptavidin conjugated to Alexa-674 (1:300; ThermoFisher S21374).

In Situ Hybridization

RNAscope Multiplex Fluorescent Reagent Kit v2 (Cat. No. 323110) was used to perform *in situ* hybridization with RNAscope probes according to company's protocols. AAV8.hSyn.DIO.EGFP was intraspinally injected into the L4/L5 segment in three CCK^{Cre} and three CR^{Cre} mice at P21, and three $VGLUT3^{Cre}$ mice at P9. The mice were perfused ten days later and the lumbar spinal cords were harvested and processed as per the manufacturer's recommended protocol for fixed frozen tissue (rather than perfused). The spinal cord segments were embedded in OCT mounting medium and cut at 20 μm using a cryostat on to SuperFrost Plus slides (Fisherbrand; Cat. No. 12-550-15). Probe combinations for the three CR^{Cre} mice were i. *Tac1*, *Lamp5* ii.*Tac2*,*Grp*. Combinations for the three CCK^{Cre} and $VGLUT3^{Cre}$ mice are as following i. *Cck* ii. *Trh* iii. *Cpne4*, *Maf*. The *Lamp5*, *Tac2*, *Cck*, *Trh* and *Maf* probes were visualized in Cy5 using the TSA® Plus multi-fluorophore detection kit (NEL760001KT). The *Tac1*, *Grp* and *Cpne4* was visualized in Cy3. Positive and negative control probes were tested on other sections simultaneously. Samples were mounted with ProLong Gold Antifade Mountant with DAPI (Thermo Fisher Scientific, Cat. No. P36931). Cells showing at least 3 puncta were considered positive.

RNA isolation, cDNA synthesis and qPCR

Mice were transcardially perfused with cold nuclease-free phosphate-buffered saline (PBS, pH. 7.4) for 2 minutes and tissues from ipsilateral L3-L5 DRGs and lumbar region of spinal cord dorsal horn were collected on day 5 after CFA and on day 7 after sural SNI. Uninjured DRGs and spinal cord tissues were used as a control. Plantar hind paw tissues were collected 2 hours after capsaicin and mustard oil injections. Plantar hind paw tissues injected with 10% ethanol in saline and mineral oil were used as a control for capsaicin and mustard oil, respectively. Tissues were rapidly collected, frozen in liquid nitrogen and stored at −80°C. Total RNA was isolated from tissue harvested in LBA buffer containing 1-Thioglycerol using ReliaPrep RNA Tissue Miniprep System (Promega, Madison, WI), and following manufacturer's protocols. Complementary DNA (cDNA) was synthesized from 500 ng of total RNA from each sample using High-Capacity cDNA Reverse Transcription Kit (Applied Biosystems, Foster City, CA) under the following conditions: 10 min at 25°C, 120 min at 37°C and 5 min at 85°C. Expression of *Cck* (59°C), *Calb2* (60°C), *Slc17a8* (60°C), *Prkcg* (60°C), *Il1b* (60°C), *Il6* (60°C), *Tnf* (60°C), *Ly6g* (60°C) and *Gapdh* (60°C) were quantified using the SsoAdvanced Universal SYBR® Green Supermix (Bio-Rad, Hercules, CA) under the following conditions: 1 cycle of 95°C for 3 min, 40 cycles of 95°C for 15 s followed by 30 s of the primer-specific annealing temperature. Primers for quantitative PCR were designed using Primer3 and NCBI Primer-BLAST and are shown in table below. All samples were run in duplicate using the CFX96 Touch Real-Time PCR system (Bio-Rad, Hercules, CA). The expression of mRNA was normalized in each sample using the *Gapdh* expression. To determine the fold change of each gene we used the ddCt method, as previously described (Livak and Schmittgen, 2001), and relative expression was compared to the control group (assigned value equal to 1).

Imaging

Spinal cord sections were imaged with a confocal laser-scanning microscope (Nikon A1R) and Nikon Elements (RRID: SCR_014329) software using 405-, 488, 561- and 640 nm excitation laser light. In order to suppress emission crosstalk, the microscope was configured to perform all scanning in sequential mode. Z series were scanned at 20x magnification with an oil immersion lens and a z-step of 5.0 μm.

Electrophysiological recordings

Young-adult mice (P25 – P35) were deeply anesthetized with 100 mg/kg ketamine and 20 mg/kg xylazine. The spinal cord was quickly removed and transferred into an ice-cold (4°C) solution containing (in mM): 220 sucrose, 2.0 KCl, 7.0 MgCl2, 26 NaHCO3, 1.15 NaH2PO4, 11 D-glucose, and 0.5 CaCl2, (pH 7.4) bubbled with 95% O2 and 5% CO2. After removing the dura mater and ventral roots, the spinal cord was embedded into 3% low-melting agarose (Fisher Scientific BP165-25) and a transverse slice (450 μm) containing L5 with the dorsal root and DRG still attached was cut using a vibroslice (Leica VT1000). The slice was incubated at 37°C in an artificial cerebrospinal fluid (aCSF) containing (in mM): 118 NaCl, 3 KCl, 2.5 CaCl2, 1.5 MgSO4, 0.6 NaH2PO4, 25 NaHCO3, 10 glucose (290-300 mOsm), pH 7.4, bubbled with 95% O2 and 5% CO2, for a 60 min recovery period. Then, the slice was transferred to a recording chamber (volume ≈1 ml) and held down with a pewter wire. The chamber was mounted on an upright microscope fitted with fluorescence optics (Carl Zeiss Axioskop 2) and linked to a Hamamatsu digital camera ORCA-R2. The slice was continuously perfused at 3.0 ml/min with the aCSF solution maintained at room temperature (≈25°C). Neurons were recorded within the inner part of lamina II that has a distinct translucent appearance and can be easily distinguished under the microscope using a X10 objective lens. Positive fluorescent neurons were visualized using a X40 water-immersion objective lens and a Cy2 or Cy3 filter set under a light delivered by a DG5 (Sutter Instruments) source. Neurons were subsequently visualized using combined infrared and differential interference.

Patch pipettes were pulled from borosilicate glass tubing (Sutter Instrument) and filled with an internal solution containing (in mM): 135 K-gluconate, 4 NaCl, 2 MgCl2, 10 HEPES, 0.2 EGTA, 2.5 ATP-Na2, 0.5 GTP-Na, Dextran Alexa 488 or Dextran Alexa-594 (0.01%) and Biocytin (0.05%) (290 mOsm), pH 7.4. Pipette resistances ranged from 5–7 MΩ. Whole-cell patch clamp recordings were acquired using an AxoPatch 200B amplifier and a Digidata 1440 digitizer (Molecular Devices) and pClamp 10.3 acquisition software (RRID: SCR_011323). Voltage clamp data were low pass filtered at 5 kHz and digitized at 10 kHz. Junction potentials were corrected before gigaseal formation. Series resistance was monitored throughout the experiments and was not compensated. Data were discarded if series resistance varied more than 20 MΩ. Voltage clamp data were recorded at a holding potential of −65 mV.

Dorsal roots were stimulated using a suction electrode at 25, 100 and 500 μA to activate Aβ or Aβ + Aδ or Aβ + Aδ + C fibers respectively at the low intensity of 0.05 Hz (duration 0.1 ms) using a A365 stimulus isolator (World Precision Instrument) as previously described (Peirs et al., 2015). At these intensities, both monosynaptic and polysynaptic EPSCs were observed. To address the monosynaptic nature of the response, the root was systematically stimulated five times at 0.05 Hz, 1 Hz, 2Hz and 20 Hz. EPSCs were considered monosynaptic in an absence of synaptic failure or latency < 2ms following a 20 Hz for Aβ fiber intensity stimulation, 2 Hz for Aδ fiber intensity stimulation and 1 Hz for C-fiber intensity stimulation as previously described (Torsney and MacDermott, 2006). Conduction velocity was systematically measured for each root stimulation. All data were analyzed offline using Axon Clampfit 10.3 software (Molecular Devices, RRID: SCR_011323).

Neuronal morphology

Slice containing $CR^{Cre/+::AAV8\text{-}hSyn\text{-}DiO\text{-}GFP}$, $CCK^{Cre/+::AAV8\text{-}hSyn\text{-}DiO\text{-}GFP}$ or $PKC\gamma^{GFP/+}$ neurons filled with 0.2% biocytin (Sigma Aldrich) for at least 20 minutes were used for neuron reconstruction. Tracer was revealed using Alexa647-conjugated streptavidin. Confocal images were taken with a 0.5 μm z-step and subsequently analyzed using Fiji-ImageJ. Single neurons were semi-automatically reconstructed using non-collapsed z stacks imported in the simple neurite tracer plug-in as previously described (Peirs et al., 2015).

QUANTIFICATION AND STATISTICAL ANALYSIS

All data are reported as mean ± SEM. For acute behaviors, a two-tailed Student's t test was used. The effect of chemogenetic activation on persistent pain behavior was analyzed by one-way repeated-measures ANOVA with Bonferroni's *Post hoc* test. The effect of PKCγ inhibitor and tat-control as well as KO and wild-type littermates were analyzed by two-way ANOVA with Bonferroni's *Post hoc* test. Comparisons of RT-PCR results were analyzed by one-way ANOVA with Bonferroni's *Post hoc* test. Significance was considered $p < 0.05$. (*$p < 0.05$, **$p < 0.01$, ***$p < 0.001$.) N = number of mice, n = number of cells or slices and are reported in the figure legends. P values (< 0.05) are reported in the figure legends. All quantitative analysis, graphs and statistical tests were performed on GraphPad Prism 8.0. Figures were made using CorelDRAW X7, GraphPad Prism 8.0, Adobe Illustrator and Adobe Photoshop CS5.5.